High-quality carnivore genomes from roadkill samples enable species delimitation in aardwolf and bat-eared fox

Rémi Allio[1*], Marie-Ka Tilak[1], Céline Scornavacca[1], Nico L. Avenant[2], Erwan Corre[3], Benoit Nabholz[1], and Frédéric Delsuc[1*]

[1]Institut des Sciences de l'Evolution de Montpellier (ISEM), CNRS, IRD, EPHE, Université de Montpellier, France remi.allio@umontpellier.fr marie-ka.tilak@umontpellier.fr celine.scornavacca@umontpellier.fr benoit.nabholz@umontpellier.fr frederic.delsuc@umontpellier.fr

[2]National Museum and Centre for Environmental Management, University of the Free State, Bloemfontein, South Africa navenant@nasmus.co.za

[3]CNRS, Sorbonne Université, FR2424, ABiMS, Station Biologique de Roscoff, 29680 Roscoff, France corre@sb-roscoff.fr

[*]Correspondence: remi.allio@umontpellier.fr, frederic.delsuc@umontpellier.fr

Abstract

In a context of ongoing biodiversity erosion, obtaining genomic resources from wildlife is becoming essential for conservation. The thousands of yearly mammalian roadkill could potentially provide a useful source material for genomic surveys. To illustrate the potential of this underexploited resource, we used roadkill samples to sequence reference genomes and study the genomic diversity of the bat-eared fox (*Otocyon megalotis*) and the aardwolf (*Proteles cristata*) for which subspecies have been defined based on similar disjunct distributions in Eastern and Southern Africa. By developing an optimized DNA extraction protocol, we successfully obtained long reads using the Oxford Nanopore Technologies (ONT) MinION device. For the first time in mammals, we obtained two reference genomes with high contiguity and gene completeness by combining ONT long reads with Illumina short reads using hybrid assembly. Based on re-sequencing data from few other roakill samples, the comparison of the genetic differentiation between our two pairs of subspecies to that of pairs of well-defined species across Carnivora showed that the two subspecies of aardwolf might warrant species status (*P. cristata* and *P. septentrionalis*), whereas the two subspecies of bat-eared fox might not. Moreover, using these data, we conducted demographic analyses that revealed similar trajectories between Eastern and Southern populations of both species, suggesting that their population sizes have been shaped by similar environmental fluctuations. Finally, we obtained a well resolved genome-scale phylogeny for Carnivora with evidence for incomplete lineage sorting among the three main arctoid lineages. Overall, our cost-effective strategy opens the way for large-scale population genomic studies and phylogenomics of mammalian wildlife using roadkill.

Keywords

Roadkill, Genomics, Population genomics, Phylogenomics, Species delimitation, Carnivora, Systematics, Genetic differentiation, Mitogenomes, Africa.

Introduction

In the context of worldwide biodiversity erosion, obtaining large-scale genomic resources from wildlife is essential for biodiversity assessment and species conservation. An underexploited but potentially useful source of material for genomics is the thousands of annual wildlife fatalities due to collisions with cars. Mammalian roadkill in particular are unfortunately so frequent that several citizen science surveys have been implemented on this subject in recent decades (Périquet et al., 2018; Shilling et al., 2015). For example, in South Africa alone, over 12,000 wildlife road mortality incidents were recorded by The Endangered Wildlife Trust's Wildlife and Roads Project from 1949 to 2017 (Endangered Wildlife Trust 2017). Initially developed to measure the impact of roads on wildlife, these web-based systems highlight the amount of car-wildlife collision. The possibility of retrieving DNA from roadkill tissue samples (Etherington et al., 2020; Maigret, 2019) could provide new opportunities in genomics by giving access not only to a large number of specimens of commonly encountered species but also to more elusive species that might be difficult to sample otherwise.

Recent advances in the development of high-throughput sequencing technologies have made the sequencing of hundreds or thousands of genetic loci cost efficient and have offered the possibility of using ethanol-preserved tissues, old DNA extracts, and museum specimens (Blaimer et al., 2016; Guschanski et al., 2013). This method combined with third generation long read sequencing technologies such as Pacific Biosciences (PacBio) and Oxford Nanopore Technologies (ONT) sequencing have increased the sizes of the sequenced molecules from several kilobases to several megabases. The relatively high level of sequencing errors (10-15%) associated with these technologies can be compensated by sequencing at a high depth of coverage to avoid sequencing errors in *de novo* genome assembly and thus obtain reference genomes with high base accuracy, contiguity, and

completeness (Koren et al., 2017; Shafin et al., 2020; Vaser et al., 2017). Originally designed to provide a portable sequencing method in the field, ONT instruments such as the MinION (Jain et al., 2016) allow direct sequencing of DNA molecules with simplified library preparation procedures even in tropical environments with elevated temperature and humidity conditions (Blanco et al., 2019; Parker et al., 2017; Pomerantz et al., 2018; Srivathsan et al., 2018). This approach is particularly suitable for sequencing roadkill specimens for which it is notoriously difficult to obtain a large amount of high-quality DNA because of post-mortem DNA degradation processes. Furthermore, it is possible to correct errors in ONT long reads by combining them with Illumina short reads, either to polish *de novo* long read-based genome assemblies (Batra et al., 2019a; Jain et al., 2018; Nicholls et al., 2019; Walker et al., 2014) or to construct hybrid assemblies (Di Genova et al., 2018; Gan et al., 2019; Tan et al., 2018; Zimin et al., 2013). In hybrid assembly approaches, the accuracy of short reads with high depth of coverage (50-100x) allows the use of long reads at lower depth of coverage (10-30x) essentially for scaffolding (Armstrong et al., 2020; Kwan et al., 2019). A promising hybrid assembly approach combining short and long read sequencing data has been implemented in MaSuRCA software (Zimin et al., 2017, 2013). This approach consists of transforming large numbers of short reads into a much smaller number of longer highly accurate “super reads” allowing the use of a mixture of read lengths. Furthermore, this method is designed to tolerate a significant level of sequencing error. Initially developed to address short reads from Sanger sequencing and longer reads from 454 Life Sciences instruments, this method has already shown promising results for combining Illumina and ONT/PacBio sequencing data in several taxonomic groups, such as plants (Scott et al., 2020; Wang et al., 2020; Zimin et al., 2017), birds (Gan et al., 2019), and fishes (Jiang et al., 2019; Kadobianskyi et al., 2019; Tan et al., 2018) but not yet in mammals.

To illustrate the potential of roadkill as a useful resource for whole genome sequencing and assembly, we studied two of the most frequently encountered mammalian roadkill species in South Africa (Périquet et al., 2018): the bat-eared fox (*Otocyon megalotis*, Canidae) and the aardwolf (*Proteles cristata,* Hyaenidae). These two species are among several African vertebrate taxa presenting disjunct distributions between Southern and Eastern African populations that are separated by more than a thousand kilometres (e.g. Ostrich (Miller et al., 2011), Ungulates Lorenzen et al. 2012). Diverse biogeographical scenarios involving the survival and divergence of populations in isolated savannah refugia during the climatic oscillations of the Pleistocene have been proposed to explain these disjunct distributions in ungulates (Lorenzen et al., 2012). Among Carnivora, subspecies have been defined based on this peculiar allopatric distribution not only for the black-backed jackal (*Canis mesomelas;* Walton and Joly 2003) but also for both the bat-eared fox (Clark, 2005) and the aardwolf (Koehler and Richardson, 1990) (**Fig. 1**). The bat-eared fox is divided into the Southern bat-eared fox (*O. megalotis megalotis*) and the Eastern bat-eared fox (*O. megalotis virgatus*) (Clark, 2005), and the aardwolf is devided into the Southern aardwolf (*P. cristata cristata*) and the Eastern aardwolf (*P. cristata septentrionalis*) (Koehler and Richardson, 1990). However, despite known differences in behaviour between subspecies within both species (Wilson et al., 2009), no genetic or genomic assessment of population differentiation has been conducted to date. In other taxa, similar allopatric distributions have led to genetic differences between populations and several studies reported substantial intraspecific genetic structuration between Eastern and Southern populations (Atickem et al., 2018; Barnett et al., 2006; Dehghani et al., 2008; Lorenzen et al., 2012; Miller et al., 2011; Rohland et al., 2005). Here we investigate whether similar genetic structuration and population differentiation have occurred between subspecies of bat-eared fox and aardwolf using whole genome data.

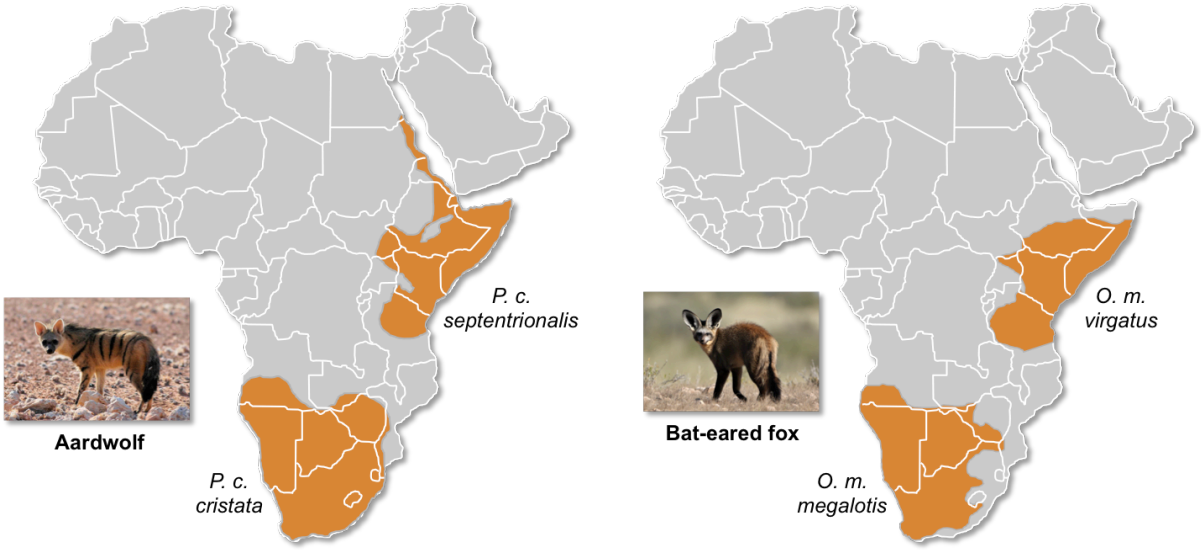

Figure 1. Disjunct distributions of the aardwolf (*Proteles cristata*) and the bat-eared fox (*Otocyon megalotis*) in Eastern and Southern Africa. Within each species, two subspecies have been recognized based on their distributions and morphological differences (Clark, 2005; Koehler and Richardson, 1990).

To evaluate the taxonomic status of the proposed subspecies within both *O. megalotis* and *P. cristata*, we first sequenced and assembled two reference genomes from roadkill samples by combining ONT long reads and Illumina short reads using the MaSuRCA hybrid assembler. The quality of our genome assemblies was assessed by comparison to available mammalian genome assemblies. Then, to estimate the genetic diversity of these species and to perform genome-scale species delimitation analyses, two additional individuals from the disjunct South African and Tanzanian populations of both species were resequenced at high depth of coverage using Illumina short reads. Using this additional population genomic data, we estimated the genetic diversity and differentiation of each subspecies pair via an FST-like measure, which we called the genetic differentiation index, and the result compared with the genetic differentiation among pairs of well-established carnivoran species. Our results indicate that the two subspecies of *P. cristata* might warrant species status whereas the two subspecies of *O. megalotis* may not. Our results showing that high-quality reference mammalian genomes could be obtained through combination of short- and long-read

sequencing methods provide opportunities for large-scale population genomic studies of mammalian wildlife using (re)sequencing of samples collected from roadkill.

Results

Mitochondrial diversity within Carnivora

The first dataset, composed of complete carnivoran mitogenomes available in GenBank combined with the newly generated sequences of the two subspecies of *P. cristata,* the two subspecies of *O. megalotis*, *Parahyaena brunnea*, *Speothos venaticus* and *Vulpes vulpes*, plus the sequences extracted from UCE libraries for *Bdeogale nigripes, Fossa fossana*, and *Viverra tangalunga*, consists of 142 species or subspecies representing all families of Carnivora. Maximum likelihood (ML) analyses reconstructed a robust mitogenomic phylogeny, with 91.4% of the nodes (128 out of 140) recovered with bootstrap support higher than 95% **(Fig. 2a)**. The patristic distances based on complete mitogenomes between the allopatric subspecies of aardwolf and bat-eared fox were 0.045 and 0.020 substitutions per site, respectively (**Table S1**). These genetic distances are comparable to those observed between different well-defined species of Carnivora such as the red fox (*Vulpes vulpes*) and the fennec (*Vulpes zerda*) (0.029) or the Steppe polecat (*Mustela eversmannii*) and the Siberian weasel (*Mustela sibirica*) (0.034) (see **Table S1**).

To further assess the genetic distances between the two pairs of subspecies and compare them to both polymorphism and divergence values observed across Carnivora, two supplemental datasets including at least two individuals per species were assembled by retrieving all COX1 and CYTB sequences, which are the two widely sequenced mitochondrial markers for carnivores, available on GenBank. These datasets include 3,657 COX1 sequences for 150 species and 6,159 CYTB sequences for 203 species of Carnivora. After adding the corresponding sequences from the newly assembled mitogenomes, ML

144 phylogenetic inference was conducted on each dataset (**Supplementary materials**). The
145 patristic distances between all tips of the resulting phylogenetic trees were measured and
146 classified into two categories: (i) intraspecific variation (polymorphism) for distances inferred
147 among individuals of the same species and (ii) interspecific divergence for distances inferred
148 among individuals of different species. Despite an overlap between polymorphism and
149 divergence in both mitochondrial genes, this analysis revealed a threshold between
150 polymorphism and divergence of apprrowimately 0.02 substitutions per site for Carnivora
151 (**Fig. 2b**). With a nucleotide distance of 0.054 for both COX1 and CYTB, the genetic
152 distance observed between the two subspecies of aardwolf (*Proteles* ssp.) was higher than the
153 majority of the intraspecific distances observed across Carnivora. However, with a nucleotide
154 distances of 0.020 for COX1 and 0.032 for CYTB, the genetic distance observed between the
155 two subspecies of bat-eared fox (*Otocyon* ssp.) was clearly in the ambiguous zone and did not
156 provide a clear indication of the specific taxonomic status of these populations.

157 Finally, to test whether the two pairs of allopatric subspecies diverged synchronously
158 or in two different time periods, Bayesian molecular dating inferences were performed on the
159 142-taxon ML mitogenomic tree. The resulting divergence times were slightly different
160 depending on the clock model used (strict clock [CL], autocorrelated [LN or TK02] and
161 uncorrelated [UGAM or UCLM]) (**Supplementary materials**). Cross-validation analyses
162 resulted in the selection of the LN and UGAM models as the models with the best fit based
163 on a higher cross-likelihood score than that of CL (LN and UGAM versus CL mean scores =
164 35 $\pm$ 8). Unfortunately, these two statistically indistinguishable models provided different
165 divergence times for the two pairs of subspecies, with LN favouring a synchronous
166 divergence (approximately 1 Mya [95% credibility interval (CI) : 6.72 - 0.43]; **Table S2**),
167 while UGAM favoured an asynchronous divergence (~0.6 [CI: 0.83 - 0.39] Mya for *O.*
168 *megalotis* ssp. and ~1.3 [CI: 1.88 - 0.93] Mya for *P. cristata* ssp.; **Table S2**). However, the

169 three chains performed with the UGAM model recovered highly similar ages for the two
170 nodes of interest with low CI 95% values whereas the three chains performed with the LN
171 model recovered less similar ages between chains and high CI 95% values (Table 1). Visual
172 inspection of the likelihood trajectories for the LN chains seems to indicate general lack of
173 convergence caused by several local optima.
174

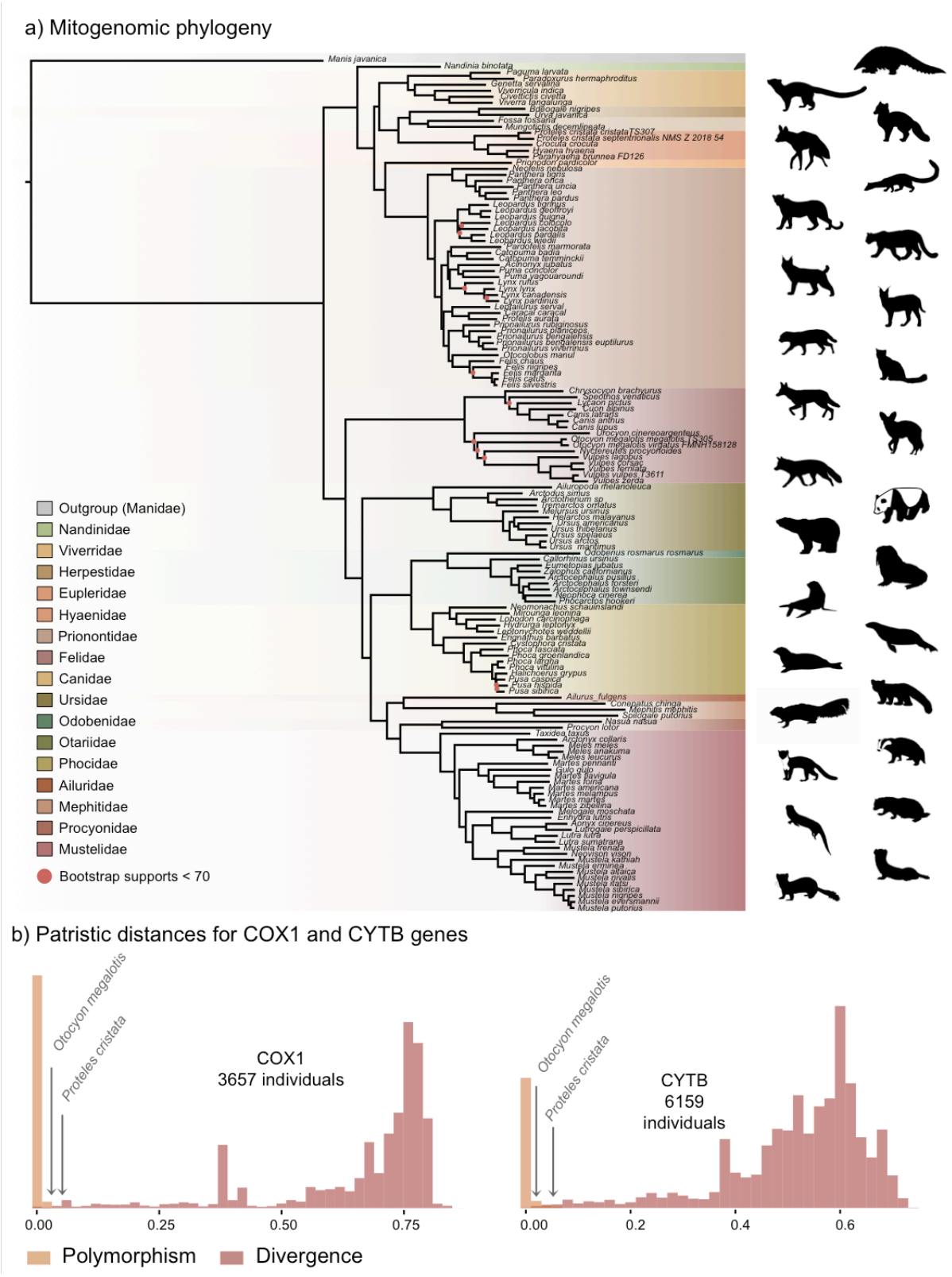

Figure 2. Representation of the mitochondrial genetic diversity within Carnivora with a) the mitogenomic phylogeny inferred from 142 complete Carnivora mitogenomes including those of the two populations of aardwolf (*Proteles cristata*) and bat-eared fox (*Otocyon megalotis*) and b) intraspecific (orange) and the interspecific (red) genetic diversities observed for the two mitochondrial markers COX1 and CYTB.

Assembling reference genomes from roadkill

Considering the DNA quality and purity required to perform single-molecule sequencing with ONT, a specific protocol to extract DNA from roadkill was developed (Tilak et al., 2020). This protocol was designed to specifically select the longest DNA fragments present in the extract also containing short degraded fragments. This protocol increased the median size of the sequenced raw DNA fragments three-fold in the case of aardwolf (Tilak et al., 2020). In total, after high-accuracy basecalling, adapter trimming, and quality filtering, 27.3 Gb of raw Nanopore long reads were sequenced using 16 MinION flow cells for the Southern aardwolf (*P. c. cristata*) and 33.0 Gb using 13 flow cells for the Southern bat-eared fox (*O. m. megalotis*) (**Table 1**). Due to quality differences among the extracted tissues for both species, the N50 of the DNA fragment size for *P. cristata* (9,175 bp) was about twice higher than the N50 of the DNA fragment size obtained for *O. megalotis* (4,393 bp). The quality of the reads basecalled with the *high accuracy* option of Guppy was significantly higher than the quality of those translated with the *fast* option, which led to better assemblies (see **Fig. S1**). Complementary Illumina sequencing returned 522.8 and 584.4 million quality-filtered reads per species corresponding to 129.5 Gb (expected coverage = 51.8x) and 154.8 Gb (expected coverage = 61.6x) for *P. c. cristata* and *O. m. megalotis*, respectively. Regarding the resequenced individuals of each species, on average 153.5 Gb were obtained with Illumina resequencing (**Table 1**).

Individuals			Illumina				Oxford Nanopore Sequencing					Assembly statistics					
Species	Subspecies	Voucher	Raw reads (M)	Cleaned reads	Nbr of gigabases	Estimated coverage	Nbr of flowcells	Nbr of bases (Gb)	N50	Average size	Estimated coverage	Genome size (Gb)	Nbr of scaff.	N50 (kb)	Busco score	OMM genes	Missing data (%)
Proteles cristata	cristata	TS307	716.7	522.8	129.50	51.8	16	27.3	9,175	5,555	10.9	2.39	5,669	1,309	92.8	12,062	22.43
Proteles cristata	cristata	TS491	663.8	526.1	140.73	56.3	NA					NA				NA	
Proteles cristata	septentrionalis	NMSZ201854	750.9	516.2	132.44	53.0										12,050	22.96
Otocyon megalotis	megalotis	TS305	710.2	584.4	154.81	61.6	13	33	4,393	3,092	13.2	2.75	11,081	728	92.9	11,981	22.02
Otocyon megalotis	megalotis	TS306	861.2	820	240.71	96.3	NA					NA					
Otocyon megalotis	virgatus	FMNH158128	661.7	554.1	100.30	40.1											

Table 1. Summary of sequencing and assembly statistics of the genomes generated in this study.

The two reference genomes were assembled using MinION long reads and Illumina short reads in combination with MaSuRCA v3.2.9 (Zimin et al., 2013). Hybrid assemblies for both species were obtained with a high degree of contiguity with only 5,669 scaffolds and an N50 of 1.3 Mb for the aardwolf (*P. cristata*) and 11,081 scaffolds and an N50 of 728 kb for the bat-eared fox (*O. megalotis*) (**Table 1**). Exhaustive comparisons with 503 available mammalian assemblies revealed a large heterogeneity among taxonomic groups and a wide variance within groups in terms of both number of scaffolds and N50 values (**Fig. 3,** **Table S3**). Xenarthra was the group with the lowest quality genome assemblies, with a median number of scaffolds of more than one million and a median N50 of only 15 kb. Conversely, Carnivora contained genome assemblies of much better quality, with a median number of scaffolds of 15,872 and a median N50 of 4.6 Mb, although a large variance was observed among assemblies for both metrics (**Fig. 3,** **Table S3**). Our two new genomes compared favourably with the available carnivoran genome assemblies in terms of contiguity showing slightly less than the median N50 and a lower number of scaffolds than the majority of the other assemblies (**Fig. 3,** **Table S3**). Comparison of two hybrid assemblies with Illumina-only assemblies obtained with SOAPdenovo illustrated the positive effect of introducing Nanopore long reads even at moderate coverage by reducing the number of scaffolds from 409,724 to 5,669 (aardwolf) and from 433,209 to 11,081 (bat-eared fox) while increasing the N50 from 17.3 kb to 1.3 Mb (aardwolf) and from 22.3 kb to 728 kb (bat-eared fox). With regard to completeness based on 4,104 single-copy mammalian BUSCO orthologues, our two hybrid assemblies are among the best assemblies with more than 90% complete BUSCO genes and less than 4% missing genes (**Fig. 4,** **Table S4**). As expected, the two corresponding Illumina-only assemblies were much more fragmented and had globally much lower BUSCO scores (**Fig. 4,** **Table S4**).

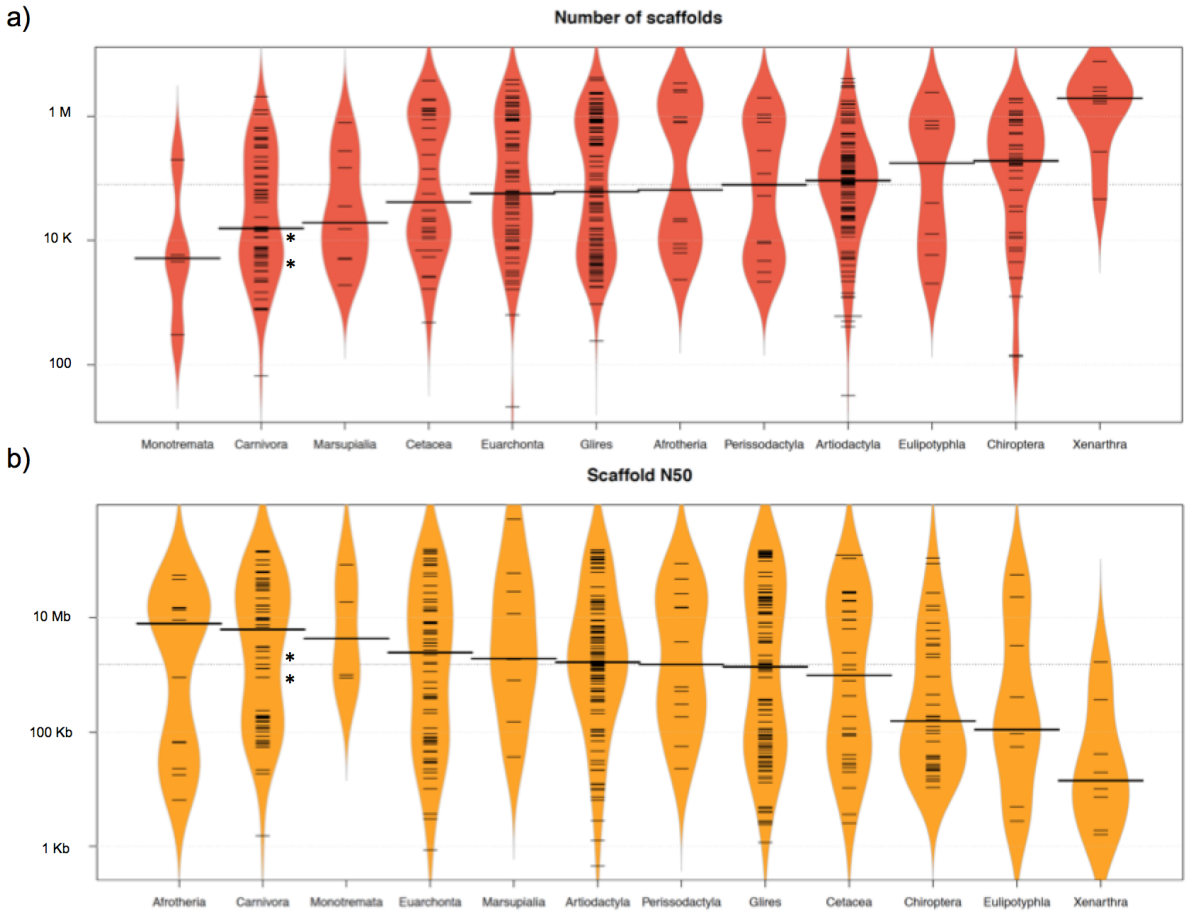

Figure 3. Comparison of 503 mammalian genome assemblies from 12 taxonomic groups using bean plots of the a) number of scaffolds, and b) scaffold N50 values ranked by median values. Thick black lines show the medians, dashed black lines represent individual data points, and polygons represent the estimated density of the data. Note the log scale of the Y axes. The bat-eared fox (*Otocyon megalotis*) and aardwolf (*Proteles cristata*) assemblies produced in this study using SOAPdenovo and MaSuRCA are indicated by asterisks. Bean plots were computed using BoxPlotR (Spitzer et al., 2014).

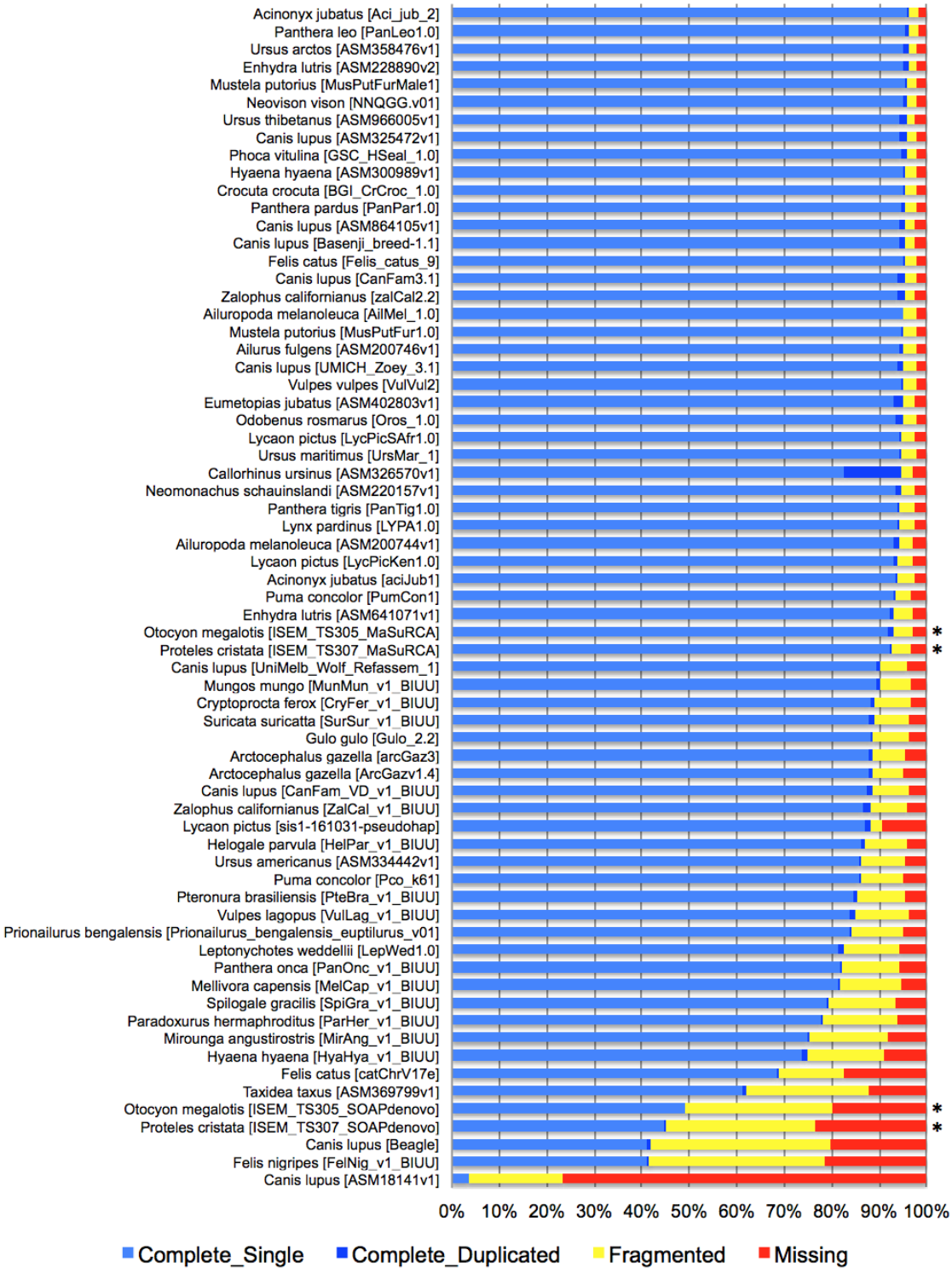

Figure 4. BUSCO completeness assessment of 67 Carnivora genome assemblies visualized as bar charts representing percentages of complete single-copy (light blue), complete duplicated (dark blue), fragmented (yellow), and missing (red) genes ordered by increasing percentage of total complete genes. The bat-eared fox (*Otocyon megalotis*) and aardwolf (*Proteles cristata*) assemblies produced in this study using MaSuRCA and SOAPdenovo are indicated by asterisks.

242 ***Genome-wide analyses of population structure***

243 To evaluate the population structure between the subspecies of *P. cristata* and *O. megalotis*,
244 the number of shared heterozygous sites, unique heterozygous sites, and homozygous sites
245 between individuals was computed to estimate an FST-like statistic (hereafter called the
246 *genetic differentiation index* or GDI). Since we were in possession of two individuals for the
247 Southern subspecies and only one for the Eastern subspecies of both species, the genetic
248 differentiation between the two individuals within the Southern subspecies and between the
249 Southern and Eastern subspecies was computed. To account for the variation across the
250 genome, 10 replicates of 100 regions with a length of 100 kb were randomly chosen to
251 estimate genetic differentiation. Interestingly, in both species, the mean heterozygosity was
252 higher in the Southern subspecies than in the Eastern subspecies. For aardwolf, the mean
253 heterozygosity was 0.189 per kb (sd = 0.010) in the Southern population and 0.121 per kb (sd
254 = 0.008) in the Eastern population. For the bat-eared fox, the mean heterozygosity was 0.209
255 per kb (sd = 0.013) in the Southern population and 0.127 per kb (sd = 0.003) in the Eastern
256 population. This heterozygosity level is low compared to those of other large mammals
257 (Diez-del-Molino et al 2018) and is comparable to that of the Iberian lynx, the cheetah or the
258 brown hyena, which have notoriously low genetic diversity (Abascal et al., 2016; Casas-
259 Marce et al., 2013; Westbury et al., 2018).

260 Since we had very limited power to fit the evolution of the genetic differentiation
261 statistics with a hypothetical demographic scenario because of our limited sample size, we
262 chose a comparative approach and applied the same analyses to four well-defined species
263 pairs of carnivorans for which similar individual sampling was available. The genetic
264 differentiation estimates between the two individuals belonging to the same subspecies
265 (Southern populations in both cases) were on average equal to 0.005 and 0.014 for *P. c.*
266 *cristata* and *O. m. megalotis*, respectively. This indicated that the polymorphism observed in

the two individuals within the Southern subspecies of each species was comparable (genetic differentiation index close to 0) and thus that these two subpopulations are likely panmictic (**Fig. 5**). In contrast, the genetic differentiation estimates for the two pairs of individuals belonging to the different subspecies were respectively equal to 0.533 and 0.294 on average for *P. cristata* ssp. and *O. megalotis* ssp., indicating that the two disjunct populations are genetically structured. To contextualize these results, the same genetic differentiation measures were estimated for four other well-defined species pairs (**Fig. 5**). First, the comparison of the polymorphism of two individuals of the same species led to intraspecific GDIs ranging from 0.029 on average for polar bear (*Ursus maritimus*) to 0.137 for lion (*Panthera leo*). As expected, comparing the polymorphisms of two individuals between closely related species led to a higher interspecific GDI ranging from 0.437 on average for the wolf/golden jackal (*Canis lupus/Canis aureus*) pair to 0.760 for the lion/leopard (*P. leo/Panthera pardus*) pair (**Fig. 5**). The genetic differentiation indices between the grey wolf (*C. lupus*) and the golden jackal (*C. aureus*) averaged 0.44, indicating that the two subspecies of aardwolf (GDI = 0.533) are genetically more differentiated than these two well-defined species, and only slightly less differentiated than the brown bear (*Ursus arctos*) and the polar bear (*U. maritimus*). Conversely, the genetic differentiation obtained between the bat-eared fox subspecies (GDI = 0.294) were lower than the genetic differentiation estimates obtained for any of the four reference species pairs evaluated here (**Fig. 5**).

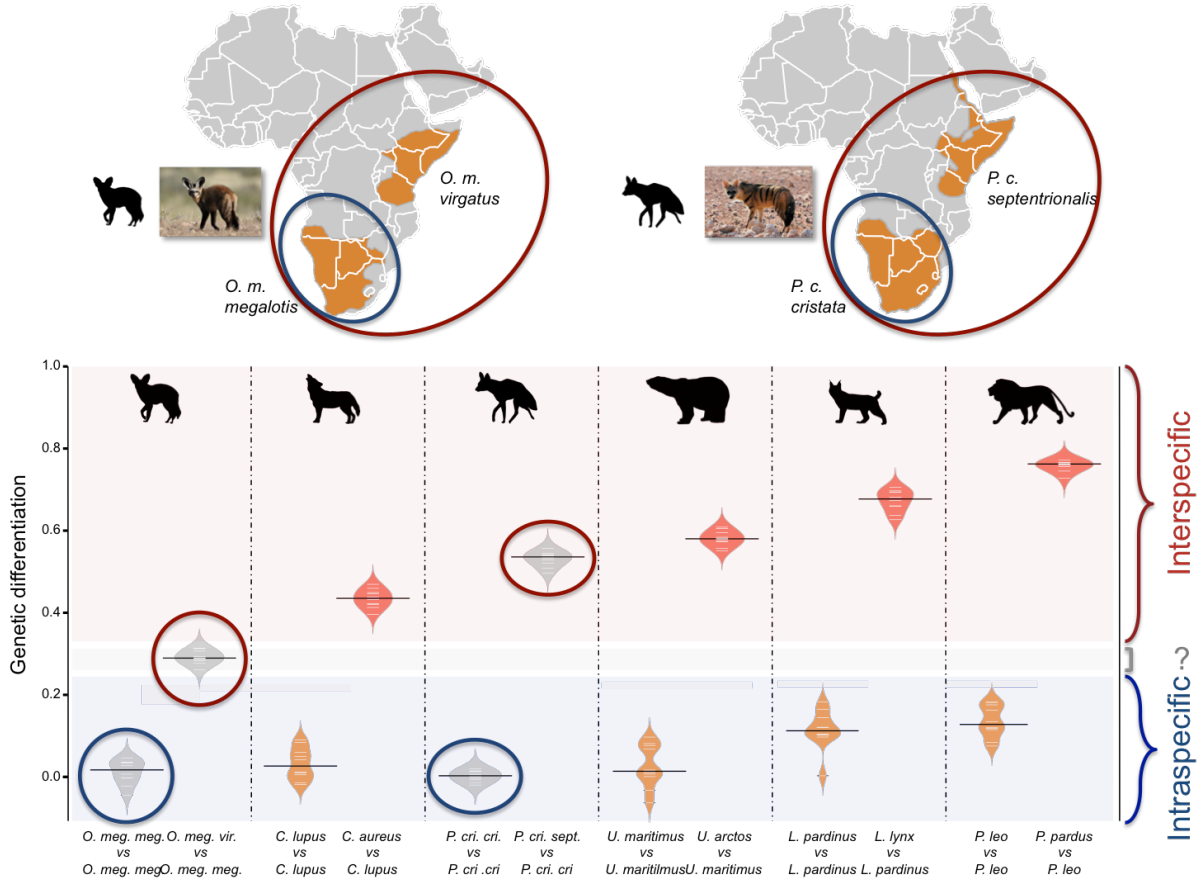

Figure 5: Genetic differentiation indices obtained from the comparison of intraspecific (orange) and interspecific (red) polymorphisms in four pairs of well-defined Carnivora species and for the subspecies of aardwolf (*Proteles cristata*) and bat-eared fox (*Otocyon megalotis*) (grey).

Effective population size reconstructions

We used the pairwise sequential Markovian coalescent (PSMC) model to estimate the ancestral effective population size (*Ne*) trajectory over time for each sequenced individual. For both the aardwolf and the bat-eared fox, the individual from Eastern African populations showed a continuous decrease in *Ne* over time, leading to the recent *Ne* being lower than that in Southern African populations (**Fig. 6**). This is in agreement with the lower heterozygosity observed in the Eastern individuals of both species. For the bat-eared fox, the trajectories of the three sampled individuals were synchronised approximately 200 kya ago (**Fig. 6a**), which could correspond to the time of divergence between the Southern and Eastern populations. In contrast, the *Ne* trajectories for the aardwolf populations did not synchronise over the whole

period (~2 Myrs). Interestingly, the Southern populations of both species showed a marked increase in population size between ~10-30 kya before sharply decreasing in more recent times (**Fig. 6**).

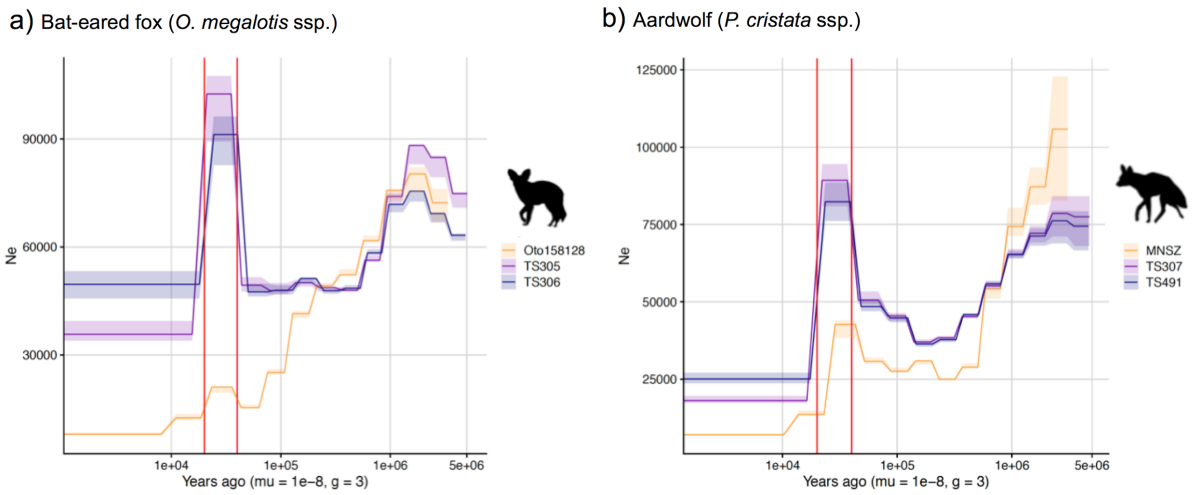

Figure 6: PSMC estimates of the change in effective population size over time for the Eastern (orange) and Southern (blue and purple) populations of a) bat-eared fox and) aardwolf. mu = mutation rate of 10^{-8} mutations per site per generation and g = generation time of 2 years. Vertical red lines indicate 20kyrs and 40kyrs.

Phylogenomics of Carnivora

Phylogenetic relationships within Carnivora were inferred from a phylogenomic dataset comprising 52 carnivoran species (including the likely new *Proteles septentrionalis* species) representing all but two families of Carnivora (Nandiniidae and Prionodontidae). The non-annotated genome assemblies of these different species were annotated with a median of 18,131 functional protein-coding genes recovered for each species. Then, single-copy orthologous gene identification resulted in a median of 12,062 out of the 14,509 single-copy orthologues extracted from the OrthoMaM database for each species, ranging from a minimum of 6,305 genes for the California sea lion (*Zalophus californianus*) and a maximum of 13,808 for the dog (*Canis lupus familiaris*) (**Table S5**). Our new hybrid assemblies allowed the recovery of 12,062 genes for the Southern aardwolf (*P. c. cristata*), 12,050 for the Eastern aardwolf (*P. c. septentrionalis*), and 11,981 for the Southern bat-eared fox (*O. m.*

megalotis) (**Table 1**). These gene sets were used to create a supermatrix consisting of 14,307 genes representing a total of 24,041,987 nucleotide sites with 6,495,611 distinct patterns (27.0%) and 22.8% gaps or undetermined nucleotides.

Phylogenomic inference was first performed on the whole supermatrix using ML. The resulting phylogenetic tree was highly supported, with all but one node being supported by maximum bootstrap (UFBS) values (**Fig. 7**). To further dissect the phylogenetic signal underlying this ML concatenated topology, we measured gene concordance (gCF) and site concordance (sCF) factors to complement traditional bootstrap node-support values. For each node, the proportion of genes (gCF) or sites (sCF) that supported the node inferred with the whole supermatrix was compared to the proportion of the genes (gDF) or sites (sDF) that supported an alternative resolution of the node (**Fig. 7**, **Supplementary materials**). Finally, a coalescent-based approximate species tree inference was performed using ASTRAL-III based on individual gene trees (**Supplementary materials**). Overall, the three different analyses provided well-supported and almost identical results (**Fig. 7**). The order Carnivora was divided into two distinct suborders: a cat-related clade (Feliformia) and a dog-related clade (Caniformia). Within Feliformia, the first split separated Felidae (felids) from Viverroidea, a clade composed of the four families Viverridae (civets and genets), Eupleridae (fossa), Herpestidae (mongooses), and Hyaenidae (hyaenas). In hyaenids, the two species of termite-eating aardwolves (*P. cristata* and *P. septentrionalis*) were the sister-group of a clade composed of the carnivorous spotted (*Crocuta crocuta*) and striped (*Hyaena hyaena*) hyenas. Congruent phylogenetic relationships among Feliformia families and within hyaenids were also retrieved with the mitogenomic data set (**Fig. 2a**). The short internal nodes of Felidae were the principal source of incongruence among the three different analyses with concordance factor analyses pointing to three nodes for which many sites and genes support alternative topologies (**Fig. 7**) including one node for which the coalescent-based

348 approximate species tree inference supported an alternative topology (**Supplementary**
349 **materials**) to the one obtained with ML on the concatenated supermatrix. In Viverroidea,
350 Viverridae split early from Herpestoidea regrouping Hyaenidae, Herpestidae, and Eupleridae,
351 within which Herpestidae and Eupleridae formed a sister clade to Hyaenidae. Within
352 Caniformia, Canidae (canids) was recovered as a sister group to Arctoidea. Within Canidae,
353 in accordance with the mitogenomic phylogeny, the Vulpini tribe, represented by *O.*
354 *megalotis* and *V. vulpes*, was recovered as the sister clade of the Canini tribe, represented
355 here by *Lycaon pictus* and *C. l. familiaris*. The Arctoidea were recovered as a major clade
356 composed of eight families grouped into three subclades: Ursoidea (Ursidae), Pinnipedia
357 (Otariidae, Odobedinae, and Phocidae), and Musteloidea, composed of Ailuridae (red
358 pandas), Mephitidae (skunks), Procyonidae (raccoons), and Mustelidae (badgers, martens,
359 weasels, and otters). Within Arctoidea, the ML phylogenetic inference on the concatenation
360 provided support for grouping Pinnipedia and Musteloidea to the exclusion of Ursidae (bears)
361 with maximum bootstrap support (**Fig. 7**), as in the mitogenomic tree (**Fig. 2a**). However, the
362 concordance factor analyses revealed that many sites and many genes actually supported
363 alternative topological conformations for this node characterized by a very short branch
364 length (sCF=34.1, SDF1=29.2, sDF2=36.7, gCF=46.9, gDF1=18.6, gDF2=18.2, gDFP=16.3)
365 (**Fig. 7**). In Pinnipedia, the clade Odobenidae (walruses) plus Otariidae (eared seals) was
366 recovered to the exclusion of Phocidae (true seals), which was also in agreement with the
367 mitogenomic scenario (**Fig. 2a**). Finally, within Musteloidea, Mephitidae represented the first
368 offshoot, followed by Ailuridae, and a clade grouping Procyonidae and Mustelidae.
369 Phylogenetic relationships within Musteloidea were incongruent with the mitogenomic tree,
370 which alternatively supported the grouping of Ailuridae and Mephitidae (**Fig. 2a**).
371

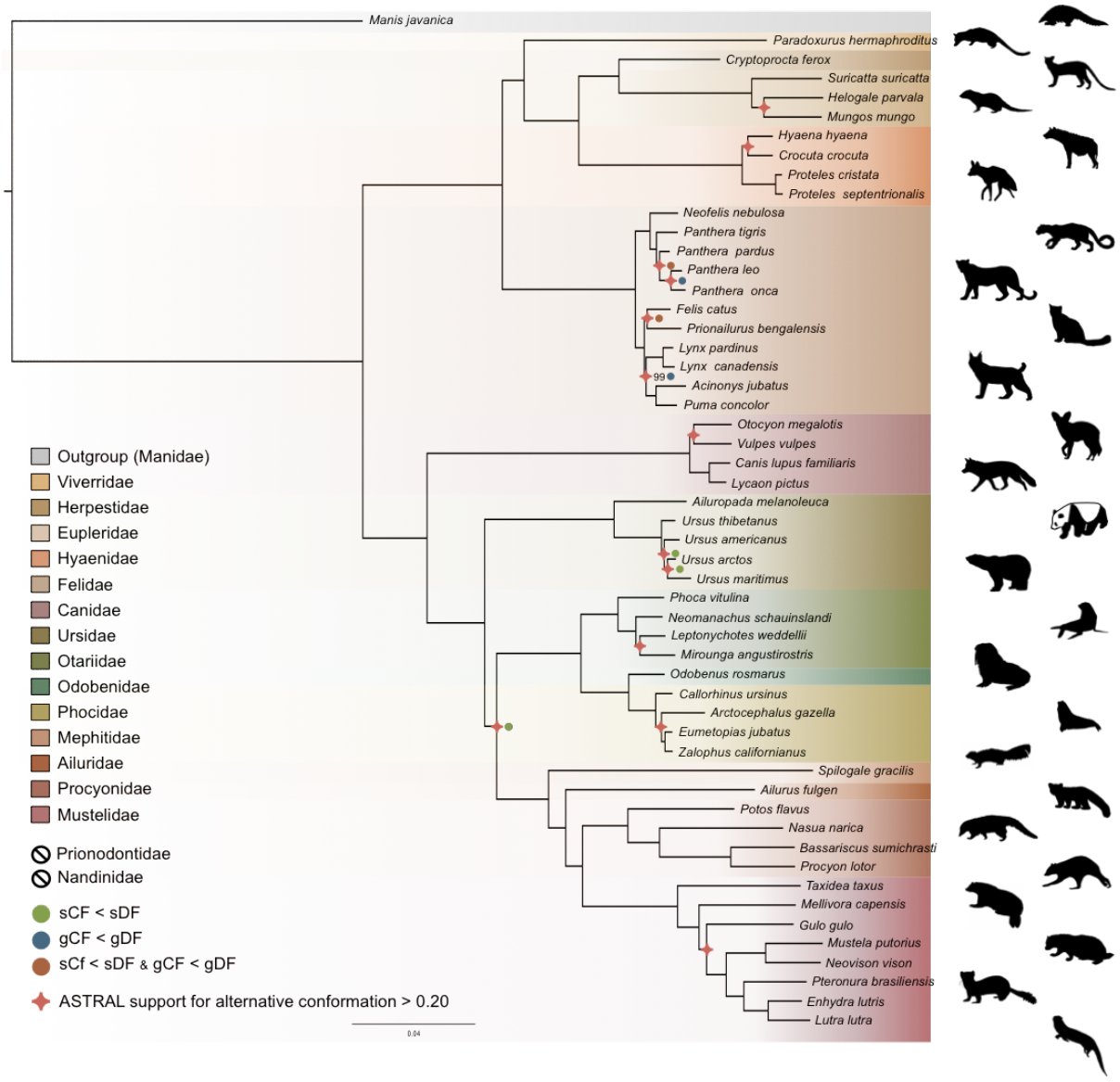

Figure 7. Phylogenomic tree reconstructed from the nucleotide supermatrix composed of 14,307 single-copy orthologous genes for 52 species of Carnivora plus one outgroup (*Manis javanica*). The family names in the legend are ordered as in the phylogeny.

Discussion

High-quality mammalian genomes from roadkill using MaSuRCA hybrid assembly

Long-read sequencing technologies and associated bioinformatic tools hold promise for making chromosome-length genome assemblies the gold standard (Dudchenko et al., 2017; Koepfli et al., 2015; Rice and Green, 2019). However, obtaining relatively large mammalian genomes of high quality remains a challenging and costly task for researchers working

outside of large genome sequencing consortia (Li et al., 2010; Lindblad-Toh et al., 2011). Despite the accuracy of short-read sequencing technologies, the use of PCR amplification is needed to increase the depth of coverage, creating uneven genomic representation and leading to sequencing biases such as GC-rich regions being less well sequenced than AT-rich ones in classical Illumina libraries (Aird et al., 2011; Tilak et al., 2018). Moreover, the use of short reads involves difficulties in the assembly of repeated regions or transposable elements longer than the sequencing read length. The use of less GC-biased long reads of single DNA molecules and ultra-long reads spanning repeated genomic regions provides a powerful solution for obtaining assemblies with high contiguity and completeness, although long-read sequencing has limited accuracy (10-20% errors). Long reads can indeed be used alone at a high depth of coverage permitting autocorrection (Koren et al., 2017; Shafin et al., 2020) or in combination with short reads for (1) scaffolding short-read contigs (Armstrong et al., 2020; Kwan et al., 2019), (2) using short reads to polish long-read contigs (Batra et al., 2019b; Datema et al., 2016; Jansen et al., 2017; Michael et al., 2018), or (3) optimizing the assembly process by using information from both long and short reads (Díaz-Viraqué et al., 2019; Gan et al., 2019; Jiang et al., 2019; Kadobianskyi et al., 2019; Tan et al., 2018; Wang et al., 2020; Zimin et al., 2017). Given the previously demonstrated efficiency of the MaSuRCA tool for the assembly of large genomes (Scott et al., 2020; Wang et al., 2020; Zimin et al., 2017), we decided to rely on hybrid sequencing data combining the advantages of Illumina short-read and Nanopore long-read sequencing technologies.

With an increasing number of species being threatened worldwide, obtaining genomic resources from mammalian wildlife can be difficult. We decided to test the potential of using roadkill samples, a currently underexploited source material for genomics (Etherington et al., 2020; Maigret, 2019). Despite limited knowledge and difficulties associated with *de novo* assembly of non-model species (Etherington et al., 2020), we designed a protocol to produce

DNA extracts of suitable quality for Nanopore long-read sequencing from roadkill (Tilak et al., 2020). Additionally, we tested the impact of the accuracy of the MinION base calling step on the quality of the resulting MaSuRCA hybrid assemblies. In line with previous studies (Wenger et al., 2019; Wick et al., 2019), we found that using the *high accuracy* option rather than the *fast* option of Guppy 3.1.5 leads to more contiguous assemblies by increasing the N50 value. By relying on this protocol, we were able to generate two hybrid assemblies by combining Illumina reads at relatively high coverage (80x) and MinION long reads at relatively moderate coverage (12x) which provides genomes with high contiguity and completeness. These represent the first two mammalian genomes obtained with such a hybrid Illumina/Nanopore approach using the MaSuRCA assembler for non-model carnivoran species: the aardwolf (*P. cristata*) and the bat-eared fox (*O. megalotis*). Despite the use of roadkill samples, our assemblies compare favourably, in terms of both contiguity and completeness, with the best carnivoran genomes obtained so far from classical genome sequencing approaches that do not rely on complementary optical mapping or chromatin conformation approaches. Overall, our carnivoran hybrid assemblies are fairly comparable to those obtained using the classic Illumina-based genome sequencing protocol involving the sequencing of both paired-end and mate-paired libraries (Li et al., 2010). The benefit of adding Nanopore long reads is demonstrated by the fact that our hybrid assemblies are of better quality than all the draft genome assemblies generated using the DISCOVAR *de novo* protocol based on a PCR-free single Illumina 250 bp paired-end library (Weisenfeld et al. 2014; DISCOVAR) used in the 200 Mammals Project of the Broad Genome Institute (The 200 mammals project).These results confirm the capacity of the MaSuRCA hybrid assembler to produce quality assemblies for large and complex genomes by leveraging the power of long Nanopore reads (Wang et al., 2020). Moreover, these two hybrid assemblies could form the basis for future chromosome-length assemblies by adding complementary HiC data (van

433 Berkum et al., 2010) as proposed in initiatives such as the Vertebrate Genome Project
434 (Koepfli et al., 2015) and DNAZoo (Dudchenko et al., 2017). Our results demonstrate the
435 feasibility of producing high-quality mammalian genome assemblies at moderate cost using
436 roadkill and should encourage genome sequencing of non-model mammalian species in
437 ecology and evolution laboratories.
438
439 ***Genomic evidence for two distinct species of aardwolves***
440 The mitogenomic distances inferred between the subspecies of *O. megalotis* and *P. cristata*
441 were comparable to those observed for other well-defined species within Carnivora.
442 Furthermore, by comparing the genetic diversity between several well-defined species
443 (divergence) and several individuals of the same species (polymorphism) based on the COX1
444 and CYTB genes across Carnivora, we were able to pinpoint a threshold of approximately
445 0.02 substitutions per base separating divergence from polymorphism, which is in accordance
446 with a recent study of naturally occurring hybrids in Carnivora (Allen et al., 2020). This
447 method, also known as the barcoding gap method (Meyer and Paulay, 2005), allowed us to
448 show that the two subspecies of *P. cristata* present a genetic divergence greater than the
449 threshold, whereas the divergence is slightly lower for the two subspecies of *O. megalotis*.
450 These results seem to indicate that the subspecies *P. c. septentrionalis* might have to be
451 elevated to the species level (*P. septentrionalis*). Conversely, for *O. megalotis*, this first
452 genetic indicator seems to confirm the distinction at the subspecies level. However,
453 mitochondrial markers have some well-identified limitations (Galtier et al., 2009), and it is
454 difficult to properly determine a threshold between polymorphism and divergence across
455 Carnivora. The measure of mtDNA sequence distances can thus be seen only as a first useful
456 indicator for species delineation. The examination of variation at multiple genomic loci in a

457 phylogenetic context, combined with morphological, behavioural and ecological data, is
458 required to establish accurate species boundaries.

459 The newly generated reference genomes allowed us to perform genome-wide
460 evaluation of the genetic differentiation between subspecies using short-read resequencing
461 data of a few additional individuals of both species. Traditionally, the reduction in
462 polymorphism in two subdivided populations (*p within*) compared to the population at large
463 (*p between*) is measured with several individuals per population (FST; Hudson et al. 1992).
464 However, given that the two alleles of one individual are the results of the combination of
465 two *a priori* non-related individuals of the population (*i.e.,* the parents), with a large number
466 of SNPs, the measurement of heterozygosity can be extended to estimation of the
467 (sub)population polymorphism. Furthermore, in a panmictic population with recombination
468 along the genome, different chromosomal regions can be considered to be independent and
469 can be used as replicates for heterozygosity estimation. In this way, genome-wide analyses of
470 heterozygosity provide a way to assess the level of polymorphism in a population and a way
471 to compare genetic differentiation between two populations. If we hypothesize that the two
472 compared populations are panmictic, picking one individual or another of the population has
473 no effect (*i.e.*, there is no individual with excess homozygous alleles due to mating preference
474 across the population), and the population structure can be assessed by comparing the
475 heterozygosity of the individuals of each population compared to the heterozygosity observed
476 for two individuals of the same population (see *Methods*). Such an index of genetic
477 differentiation, by measuring the level of population structure, could provide support to
478 establish accurate species boundaries. In fact, delineating species has been and still is a
479 complex task in evolutionary biology (Galtier, 2019; Ravinet et al., 2016; Roux et al., 2016).
480 Given that accurately defining the species taxonomic level is essential for a number of
481 research fields, such as macroevolution (Faurby et al., 2016) or conservation (Frankham et

al., 2012), defining thresholds to discriminate between populations or subspecies in different species is an important challenge in biology. However, due to the disagreement on the definition of species, the different routes of speciation observed *in natura* and the different amount of data available among taxa, adapting a standardized procedure for species delineation seems complicated (Galtier, 2019).

As proposed by Galtier (Galtier, 2019), we decided to test the taxonomic level of the *P. cristata* and *O. megalotis* subspecies by comparing the genetic differentiation observed between Eastern and Southern populations within these species to the genetic differentiation measured for well-defined Carnivora species. Indeed, estimation of the genetic differentiation either within well-defined species (polymorphism) or between two closely related species (divergence) allowed us to define a threshold between genetic polymorphism and genetic divergence across Carnivora (**Fig. 5**). Given these estimates, and in accordance with mitochondrial data, the two subspecies of *P. cristata* (1) present more genetic differentiation between each other than the two well-defined species of golden jackal (*Canis aureus*) and wolf (*Canis lupus*), and (2) present more genetic differentiation than the more polymorphic species of the dataset, the lion (*P. leo*). Despite known cases of natural hybridization reported between *C. aureus* and *C. lupus* (Galov et al., 2015; Gopalakrishnan et al., 2018), the taxonomic rank of these two species is well accepted. In that sense, given the species used as a reference, the two subspecies of *P. cristata* seem to deserve to be elevated to the species level. The situation is less clear regarding the subspecies of *O. megalotis*. Indeed, while the genetic differentiation observed between the two subspecies is significantly higher than the polymorphic distances observed for all the well-defined species of the dataset, there is no species in our dataset that exhibits equivalent or lower genetic divergence than a closely related species. This illustrates the limits of delineating closely related species due to the continuous nature of the divergence process (De Queiroz, 2007). The subspecies of *O.*

megalotis fall into the "grey zone" of the speciation continuum (De Queiroz, 2007; Roux et al., 2016) and are likely undergoing speciation due to their vicariant distributions. To be congruent with the genetic divergence observed across closely related species of Carnivora (according to our dataset), we thus propose that (1) the taxonomic level of the *P. cristata* subspecies be reconsidered by elevating the two subspecies *P. c. cristata* and *P. c. septentrionalis* to the species level, and (2) the taxonomic level for the two subspecies of *O. megalotis* be maintained. These new taxonomic results should prompt a deeper investigation of morphological and behavioural differences that have been reported between the two proposed subspecies of aardwolf to formally validate our newly proposed taxonomic arrangement. They also have conservation implications, as the status of the two distinct aardwolf species will have to be re-evaluated separately in the International Union for Conservation of Nature (IUCN) Red List of Threatened Species (IUCN 2020, 2020).

Population size variation and environmental change

The Pairwise Sequentially Markovian Coalescent (PSMC) analyses revealed that the Southern and Eastern African populations have different effective population size estimates over time, confirming that they have been genetically isolated for several thousand years, which is more so for the aardwolf than for the bat-eared fox. This supports the hypothesis of two separate events leading to the same disjunct repartitions for the two taxa, in accordance with mitochondrial dating. Nevertheless, the population trends are rather similar and are characterized by continuous declines between 1 Mya and 100-200 kya that are followed by an increase that is much more pronounced in the Southern populations of both species between 30-10 kya. The similar trajectories exhibited by both species suggest that they were under the influence of similar environmental factors, such as climate and vegetation variations.

Aardwolves and bat-eared foxes live in open environments including short-grass plains, shrubland, and open and tree savannahs, and both are highly dependent on herbivorous termites for their diet. Therefore, the fluctuation of their populations could reflect the evolution of these semi-arid ecosystems determining prey abundance during the last million years. However, the global long-term Plio-Pleistocene African climate is still debated. For Eastern Africa, some studies have suggested an evolution towards increased aridity (deMenocal, 2004, 1995) whereas others have proposed the opposite (Grant et al., 2017; Maslin et al., 2014; Trauth et al., 2009). Our data therefore support the latter hypothesis, as a global long-term tendency towards a wetter climate in East Africa could have been less favourable for species living in open environments.

Southern populations exhibit a similar decreasing trend between 1 Mya and 100 kya. Once again, the relevant records appear contradictory. This could be the result of regional variation across South Africa, with aridification in the Southwestern part and wetter conditions in the Southeast (Caley et al., 2018; Johnson et al., 2016). Finally, the 30-10 kya period appears to have been more humid (Chase et al., 2019; Chevalier and Chase, 2015; Lim et al., 2016). This seems inconsistent with the large population increase detected in Southern populations of both species; however, the large regions of the Namib Desert that are currently unsuitable could have been more favorable in wetter conditions.

The global decrease in population size detected in the Southern and Eastern populations could also reflect the fragmentation of a continuous ancestral range. The global trend towards a wetter climate may have favoured the development of the tropical rainforest in central Africa creating a belt of unsuitable habitat. This is in line with previous studies describing diverse biogeographical scenarios involving the survival and divergence of ungulate populations in isolated savannah refuges during Pleistocene climate oscillations (Lorenzen et al., 2012). In this respect, it could be interesting to study population trends in

556 other species living in semi-arid environments and having a similar range as disconnected
557 populations. Interestingly, several bird species also have similar distributions including the
558 Orange River francolin (*Scleroptila gutturalis*), the greater kestrel (*Falco rupicoloides*), the
559 double-banded courser (*Smutsornis africanus*), the red-fronted tinkerbird (*Pogoniulus*
560 *pusillus*), the cape crow (*Corvus capensis*) and the black-faced waxbill (*Estrilda*
561 *erythronotos*), supporting the role of the environment in the appearance of these disjunct
562 repartitions. Finally, these new demographic results showing recent population size declines
563 in both regions in both species might be taken into account when assessing the conservation
564 status of the two distinct aardwolf species and bat-eared fox subspecies.
565
566 ***Genome-scale phylogeny of Carnivora***
567 In this study, we provide a new phylogeny of Carnivora including the newly recognized
568 species of aardwolf (*P. septentrionalis*). The resulting phylogeny is fully resolved with all
569 nodes supported with UFBS values greater than 95% and is congruent with previous studies
570 (Doronina et al., 2015; Eizirik et al., 2010) (**Fig. 5**). Across Carnivora, the monophyly of all
571 superfamilies described are strongly supported (Flynn et al., 2010) and are divided into two
572 distinct suborders: a cat-related clade (Feliformia) and a dog-related clade (Caniformia). On
573 the one hand, within Feliformia, the different families and their relative relationships are well
574 supported and are in accordance with previous studies (Eizirik et al., 2010). There is one
575 interesting point regarding the Felidae family. While almost all the nodes of the phylogeny
576 were recovered as strongly supported from the three phylogenetic inference analyses (ML
577 inferences, concordance factor analyses and coalescent-based inferences), one third of the
578 nodes (3 out of 9) within Felidae show controversial node supports. This result is not
579 surprising and is consistent with previous studies arguing for ancient hybridization among
580 Felidae (Li et al., 2016). Another interesting point regarding Feliformia and particularly

Hyaenidae is the relationship of the two aardwolves. The two species, *P. cristasta* and *P. septentrionalis* form a sister clade to the clade composed of the striped hyena (*H. hyaena)* and the spotted hyena (*C. crocuta),* in accordance with previous studies (Koepfli et al., 2006; Westbury et al., 2018) and the two subfamilies Protelinae and Hyaeninae that have been proposed for these two clades, respectively. However, although the phylogenetic inferences based on the supermatrix of 14,307 single-copy orthologues led to a robust resolution of this node according to the bootstrap supports, both concordance factors and coalescent-based analyses revealed conflicting signals with support for alternative topologies. In this sense, the description and acceptance of the Hyaninae and Protelinae families still require further analyses, and including genomic data for the brown hyena (*Parahyena brunnea*) seems essential (Westbury et al., 2018).

On the other hand, within Caniformia, the first split separates Canidae from the Arctoidea. Within Canidae, the bat-eared fox (*O. megalotis)* is grouped with the red fox (Vulpes vulpes), the other representative of the tribe Vulpini, but with a very short branch and concordance analyses indicating conflicting signals on this node. Regarding Arctoidea, historically, the relationships between the three superfamilies of arctoids have been contradictory and debated. The least supported scenario from the litterature is that in which the clade Ursoidea/Musteloidea is a sister group of Pinnipedia (Flynn and Nedbal, 1998). Based on different types of phylogenetic characters, previous studies found support for both the clade Ursoidea/Pinnipedia (Agnarsson et al., 2010; Meredith et al., 2011; Rybczynski et al., 2009) and the clade Pinnipedia/Musteloidea (Arnason et al., 2007; Eizirik et al., 2010; Flynn et al., 2005; Sato et al., 2009, 2006; Schröder et al., 2009). However, investigations of the insertion patterns of retroposed elements revealed the occurrence of incomplete lineage sorting (ILS) at this node (Doronina et al., 2015). With a phylogeny inferred from 14,307 single-copy orthologous genes, our study, based on both gene trees and supermatrix

606 approaches, gives support to the variant Pinnipedia/Musteloidea excluding Ursoidea as the
607 best supported conformation for the Arctoidea tree (Doronina et al., 2015; Eizirik et al., 2010;
608 Sato et al., 2006). Interestingly, in agreement with Doronina et al. (Doronina et al., 2015), our
609 concordance factor analysis supports the idea that the different conformations of the
610 Arctoidea tree are probably due to incomplete sorting of the lineage by finding almost the
611 same number of sites supporting each of the three conformations (34.11%, 29.61% and
612 36.73%). However, although trifurcation of this node is supported by these proportions of
613 sites, a majority of genes taken independently (gene concordance factors: 6,624 out of 14,307
614 genes) and the coalescent-based species tree approach (quartet posterior probabilities q1 =
615 0.53, q2 = 0.24, q3 = 0.24) support the clade Pinnipedia/Musteloidea excluding Ursoidea.
616 Considering these results, the difficulty of resolving this trifurcation among Carnivora
617 (Delisle and Strobeck, 2005) has likely been contradictory due to the ILS observed among
618 these three subfamilies (Doronina et al., 2015), which led to different phylogenetic scenarios
619 depending on the methods (Peng et al., 2007) or markers (L and YP, 2006) used. Another
620 controversial point, likely due to incomplete lineage sorting (Doronina et al., 2015) within the
621 Carnivora phylogeny, is the question regarding which of Ailuridae and Mephitidae is the
622 most basal family of the Musteloidea (Doronina et al., 2015; Eizirik et al., 2010; Flynn et al.,
623 2005; Sato et al., 2009). Interestingly, our phylogenetic reconstruction based on mitogenomic
624 data recovered the clade Ailuridae/Mephitidae as a sister clade of all other Musteloidea
625 families. The phylogenomic inferences based on the genome-scale supermatrix recovered the
626 Mephitidae family as the most basal family of Musteloidea. This result is supported by both
627 coalescent-based inferences and concordance factors. In that sense, despite incomplete
628 lineage sorting (Doronina et al., 2015), at the genomic level, it seems that the Mephitidae
629 family would be the most basal family of Musteloidea.

630 Overall, the phylogenomic inference based on 14,307 single-copy orthologous genes
631 provides a new vision of the evolution of Carnivora. The addition of information from both
632 concordance factor analyses (Minh et al., 2020) and coalescent-based inference (Zhang et al.,
633 2018) supports previous analyses showing controversial nodes in the Carnivora phylogeny.
634 Indeed, this additional information seems essential in phylogenomic analyses based on
635 thousands of markers, which can lead to highly resolved and well-supported phylogenies
636 despite support for alternative topological conformations for controversial nodes (Allio et al.,
637 2020b; Jeffroy et al., 2006; Kumar et al., 2012).
638

639 ## Conclusions

640 The protocol developed here to extract the best part of the DNA from roadkill samples
641 provides a good way to obtain genomic data from wildlife. Combining Illumina sequencing
642 data and Oxford Nanopore long-read sequencing data using the MaSuRCA hybrid assembler
643 allowed us to generate high-quality reference genomes for the Southern aardwolf (*P. cristata*)
644 and the Southern bat-eared fox (*O. megalotis megalotis*). This cost-effective strategy provides
645 opportunities for large-scale population genomic studies of mammalian wildlife using
646 resequencing of samples collected from roadkill. Indeed, by defining a genetic differentiation
647 index based on only three individuals, we illustrate the potential of the approach for genome-
648 scale species delineation in both species for which subspecies have been defined based on
649 disjunct distributions and morphological differences. Our results, based on both
650 mitochondrial and nuclear genome analyses, indicate that the two subspecies of *P. cristata*
651 warrant elevation to the species taxonomic level; the *O. megalotis* subspecies do not warrant
652 this status, but are likely ongoing species. Hence, by generating reference genomes with high
653 contiguity and completeness, this study shows a concrete application for genomics of roadkill
654 samples.

Methods

Biological samples

We conducted fieldwork in the Free State province of South Africa in October 2016 and October 2018. While driving along the roads, we opportunistically collected tissue samples from four roadkill specimens from which we sampled ear necropsies preserved in 95% Ethanol: two bat-eared foxes (O. megalotis NMB TS305, GPS: 29°1'52"S, 25°9'38"E and NMB TS306, GPS: 29°2'33"S, 25°10'26"E), and two aardwolves (P. cristata NMB TS307, GPS: 29°48'45"S, 26°15'0"E and NMB TS491, GPS: 29°8'42"S, 25°39'4"E). As aardwolf specimen NMB TS307 was still very fresh, we also sampled muscle and salivary gland necropsies preserved in RNAlater™ stabilization solution (Thermo Fisher Scientific). These roadkill specimens have been sampled under standing collecting permit number S03016 issued by the Department of National Affairs in Pretoria (South Africa) granted to the National Museum, Bloemfontein. These samples have been sent to France under export permits (JM 3007/2017 and JM 5043/2018) issued by the Free State Department of Economic, Small Business Development, Tourism and Environmental Affairs (DESTEA) in Bloemfontein (Free State, South Africa) and import permits issued by the Direction régionale de l'environnement, de l'aménagement et du logement (DREAL) Occitanie in Toulouse (France). All tissue samples collected in this study have been deposited in the mammalian tissue collection of the National Museum, Bloemfontein (Free State, South Africa).

Mitochondrial barcoding and phylogenetics

Mitogenomic dataset construction

In order to assemble a mitogenomic data set for assessing mitochondrial diversity among *P. cristata* and *O. megalotis* subspecies, we generated seven new Carnivora mitogenomes using

Illumina shotgun sequencing (**Table S6**). Briefly, we extracted total genomic DNA total using the DNeasy Blood and Tissue Kit (Qiagen) for *P. c. cristata* (NMB TS307), *P. c. septentrionalis* (NMS Z.2018.54), *O. m. megalotis* (NMB TS305), *O. m. virgatus* (FMNH 158128), *Speothos venaticus* (ISEM T1624), *Vulpes vulpes* (ISEM T3611), and *Parahyaena brunnea* (ISEM FD126), prepared Illumina libraries following the protocol of Tilak et al. (Tilak et al., 2015), and sent libraries to the Montpellier GenomiX platform for single-end 100 bp sequencing on a Illumina HiSeq 2500 instrument to obtain about 5 to 10 million reads per sample. We then assembled and annotated mitogenomes from these single-read shotgun sequencing data with MitoFinder v1.0.2 (Allio et al., 2020a) using default parameters. We also used MitoFinder to extract three additional mitogenomes from paired-end Illumina capture libraries of ultra-conserved elements (UCEs) and available from the Short Read Archive (SRA) of NCBI for *Viverra tangalunga*, *Bdeogale nigripes*, and *Fossa fossana* Additional read mappings were done with Geneious (Kearse et al., 2012) to close gaps when the mitochondrial genome was fragmented. Finally, we downloaded all RefSeq carnivoran mitogenomes available in Genbank (135 species as of July 1st, 2019) and the mitogenome of the Malayan pangolin (*Manis javanica*) to use as outgroup.

Mitogenomic phylogenetics and dating

Mitochondrial protein coding genes were individually aligned using MACSE v2 (Ranwez et al., 2018) with default parameters, and ribosomal RNA genes using MAFFT (Katoh and Standley, 2013) algorithm FFT-NS-2 with option --*adjustdirection*. A nucleotide supermatrix was created by concatenating protein-coding and ribosomal RNA genes for the 142 taxa (140 species and 2 subspecies). Phylogenetic inferences were performed with Maximum likelihood (ML) as implemented in IQ-TREE 1.6.8 (Nguyen et al., 2014) with the GTR+G4+F model. Using the resulting topology, divergence time estimation was performed using Phylobayes v4.1c (Lartillot et al., 2013) with strict clock (CL), autocorrelated (LN or

705 TK02), and uncorrelated (UGAM or UCLM) models combined with 18 fossil calibrations
706 (**Table S7**). Three independent Markov chains Monte Carlo (MCMC) analyses starting from
707 a random tree were run until 10,000 generated cycles with trees and associated model
708 parameters sampled every cycle. A burn-in of 25% was applied before constructing the
709 majority-rule Bayesian consensus tree with the *readdiv subprogram*. Finally, to determine the
710 best-fitting clock model, cross-validation analyses were performed with Phylobayes by
711 splitting the dataset randomly into two parts. Then, parameters of one model were estimated
712 on the first part of the dataset (here representing 90%) and the parameter values were used to
713 compute the likelihood of the second part of the dataset (10%). This procedure was repeated
714 ten times for each model. Finally, the likelihood of each repeated test was computed and
715 summed for each model with the *readcv* and *sumcv* subprograms, respectively. The molecular
716 clock model with the highest cross-likelihood scores was considered as the best fitting.

717 *Mitochondrial diversity and barcoding gap analyses*

718 To check if a threshold between intraspecific variation and interspecific divergence could be
719 determined across Carnivora (Meyer and Paulay, 2005), two mitochondrial barcoding
720 datasets were assembled from all COX1 and CYTB sequences available for Carnivora plus
721 the corresponding sequences for the two subspecies of *O. megalotis* and *P. cristata*,
722 respectively. After aligning each barcoding dataset with MACSE v2, ML phylogenetic
723 inferences were performed with IQ-TREE 1.6.6 using the optimal substitution model as
724 determined by ModelFinder (Kalyaanamoorthy et al., 2017). Then, pairwise patristic
725 distances between all individuals were calculated from the resulting ML phylogram. Finally,
726 based on the actual taxonomic assignment, patristic distances were considered as intraspecific
727 variation between two individuals belonging to the same species and as interspecific
728 divergence between individuals of different species.

729

730 **Short reads and long reads hybrid assembly of reference genomes**

731 *Sampling*

732 To construct reference assemblies with high contiguity for the two focal species we selected
733 the best-preserved roadkill samples: NMB TS305 for *O. megalotis* and NMB TS307 for *P.*
734 *cristata* (Table 1). Total genomic DNA extractions were performed separately for Illumina
735 short-read sequencing and MinION long-read sequencing.

736 *Illumina short-read sequencing*

737 Total genomic DNA extractions were performed from ear necropsies for the two sampled
738 individuals using the DNeasy Blood and Tissue Kit (Qiagen) following manufacturer's
739 instructions. A total amount of 1.0µg DNA per sample was sent as input material for Illumina
740 library preparation and sequencing to Novogene Europe (Cambridge, UK). Sequencing
741 libraries were generated using NEBNext® DNA Library Prep Kit following manufacturer's
742 recommendations and indices were added to each sample. Genomic DNA was randomly
743 fragmented to a size of 350bp by shearing, then DNA fragments were end-polished, A-tailed,
744 and ligated with the NEBNext adapter for Illumina sequencing, and further PCR enriched by
745 P5 and indexed P7 oligos. The PCR products were purified (AMPure XP system) and the
746 resulting libraries were analysed for size distribution by Agilent 2100 Bioanalyzer and
747 quantified using real-time PCR. Since the genome sizes for these two species was estimated
748 to be about 2.5 Gb, Illumina paired-end 250 bp sequencing was run on HiSeqX10 and
749 NovaSeq instruments to obtain about 200 Gb per sample corresponding to a genome depth of
750 coverage of about 80x.

751

752 *MinION long-read sequencing*

753 Considering the DNA quality required to perform sequencing with Oxford Nanopore
754 Technologies (ONT), a specific protocol to extract DNA from roadkill was designed (Tilak et

al., 2020). First, genomic DNA was extracted by using the classical Phenol-chloroform method. Then, we evaluated the cleanliness of the extractions by using (1) a binocular magnifying glass to check the absence of suspended particles (e.g. hairpieces), and (2) both Nanodrop and Qubit/Nanodrop ratio. To select the longest DNA fragments, we applied a specific ratio of 0.4x of AMPure beads applied (Tilak et al., 2020). Extracted-DNA size was then homogenized using covaris G-tubes. Finally, long-read ONT sequencing was performed through MinION flowcells (FLO-MIN-106) using libraries prepared with the ONT Ligation Sequencing kit SQK-LSK109. For both species, we run MinION sequencing until about 30 Gb per sample were obtained to reach a genome depth of coverage of about 12x.

Hybrid assembly of short and long reads

Short reads were cleaned using Trimmomatic 0.33 (Bolger et al., 2014) by removing low quality bases from their beginning (LEADING:3) and end (TRAILING:3), by removing reads shorter than 50 bp (MINLEN:50). Quality was measured for sliding windows of four base pairs and had to be greater than 15 on average (SLIDINGWINDOW:4:15). For MinION sequencing, base calling of fast5 files were performed using Guppy v3.1.5 (developed by ONT) with the *high accuracy* option, which is longer but more accurate than the standard *fast* model (**Fig. S1**). Long read adapters were removed using Porechop v0.2.3 (https://github.com/rrwick/Porechop). To take advantage of both the high accuracy of Illumina short reads sequencing and the size of MinION long reads, assemblies were performed using the MaSuRCA hybrid genome assembler (Zimin et al., 2013). This method transforms large numbers of paired-end reads into a much smaller number of longer 'super-reads' and permits assembling Illumina reads of differing lengths together with longer ONT reads. To illustrate the advantage of using short reads and long reads conjointly, assemblies were also performed with short reads only using SOAP-denovo (Luo et al., 2012) (kmer size=31, default parameters) and gaps between contigs were closed using the abundant paired

780 relationships of short reads with GapCloser 1.12 (Luo et al., 2012). To evaluate genome
781 quality, traditional measures like the number of contigs, the N50, the mean and maximum
782 length were evaluated for 503 mammalian genome assemblies retrieved from NCBI
783 (https://www.ncbi.nlm.nih.gov/assembly) on August 13th, 2019 with filters: "Exclude
784 derived from surveillance project", "Exclude anomalous", "Exclude partial", and using only
785 the RefSeq assembly for *Homo sapiens*. Finally, we assessed the gene completeness of our
786 assemblies by comparison with the 63 carnivoran assemblies available at NCBI on August
787 13th, 2019 using Benchmarking Universal Single-Copy Orthologs (BUSCO) v3 (Waterhouse
788 et al., 2018) with the Mammalia OrthoDB 9 BUSCO gene set (Zdobnov et al., 2017) through
789 the gVolante web server (Nishimura et al., 2017).
790
791 **Species delimitation based on genomic data**
792 *Sampling and resequencing*
793 To assess the genetic diversity in *P. cristata*, we sampled an additional roadkill individual of
794 the South African subspecies *P. c. cristata* (NMB TS491) and an individual of the East
795 African subspecies *P. c. septentrionalis* (NMS Z.2018.54) from Tanzania (**Table 1; Table**
796 **S6**). A similar sampling was done for *O. megalotis*, with an additional roadkill individual of
797 the South African subspecies *O. m. megalotis* (NMB TS306) and an individual of the East
798 African subspecies *O. m. virgatus* (FMNH 158128) from Tanzania (**Table 1; Table S6**).
799 DNA extractions were performed with the DNeasy Blood and Tissue Kit (Qiagen), following
800 manufacturer's instructions and a total amount of 1.0µg DNA per sample was outsourced to
801 Novogene Europe (Cambridge, UK) for Illumina library preparation and Illumina paired-end
802 250 bp sequencing on HiSeqX10 and NovaSeq instruments to obtain about 200 Gb per
803 sample (genome depth of coverage of about 80x). The resulting reads were cleaned using
804 Trimmomatic 0.33 with the same parameters as described above.

Heterozygosity and genetic differentiation estimation

In a panmictic population, alleles observed in one individual are shared randomly with other individuals of the same population and the frequencies of homozygous and heterozygous alleles should follow Hardy-Weinberg expectations. However, a structuration in subpopulations leads to a deficiency of heterozygotes (relative to Hardy-Weinberg expectations) in these subpopulations due to inbreeding (Holsinger and Weir, 2009; Walhund, 2010) and thus decreases the polymorphism within the inbred subpopulations with respect to the polymorphism of the global population. Given that, Hudson et al. (Hudson et al., 1992) defined the FST as a measure of polymorphism reduction in two subdivided populations (*p within*) compared to the population at large (*p between*).

To assess the *p within* and *p between* of the two subspecies of each species (*P. cristata* and *O. megalotis*), we compared the heterozygous alleles (SNPs) of two individuals of the same subspecies and the SNPs of two individuals of different subspecies by computing a FST-like statistic (hereafter called Genetic Differentiation Index: GDI) (Fig. S2). In fact, polymorphic sites can be discriminated in four categories: (1) fixed in one individual (*e.g.* AA/TT); (2) shared with both individuals (*e.g.* AT/AT); (3) specific to individual 1 (*e.g.* AT/AA); and (4) specific to individual 2 (*e.g.* AA/AT). Using these four categories, it is possible to estimate the polymorphism of each individual 1 and 2 and thus estimate a GDI between two individuals of the same population A and the GDI between two individuals of different populations A and B as follows:

$$GDI\ intra\ A = 1 - \frac{(\pi A1 + \pi A2) / \pi A2}{\pi\ tot\ A} \quad \text{and} \quad GDI\ intra\ B = 1 - \frac{(\pi B1 + \pi B2) / \pi B2}{\pi\ tot\ B}$$

For each species, cleaned short reads of all individuals (the one used to construct the reference genome and the two resequenced from each population) were aligned with their

reference genome using BWA-MEM (Li, 2013). BAM files were created and merged using SAMtools (Li et al., 2009). Likely contaminant contigs identified using BlobTools (Laetsch and Blaxter, 2017) (**Fig. S3, Tables S8-S9**) and contigs belonging to the X chromosome following BLASTN annotation (-perc_identity 80%, -evalue 10e-20) were removed. Then, 100 regions of 100,000 bp were randomly sampled among contigs longer than 100,000 bp and 10 replicates of this sampling were performed (*i.e.* 10 x 100 x 100,000 bp = 100 Mb) to assess statistical variance in the estimates. Genotyping of these regions was performed with freebayes v1.3.1-16 (git commit id: g85d7bfc) (Garrison and Marth, 2012) using the parallel mode (Tange, 2011). Only SNPs with freebayes-estimated quality higher than 10 were considered for further analyses. A first GDI estimation comparing the average of the private polymorphisms of the two southern individuals (*p within A*) and the total polymorphism of the two individuals (*p between A*) was estimated to control that no genetic structure was observed in the Southern subspecies. Then a global GDI comparing the private polymorphisms of individuals from the two populations (*p within AB*) and the total polymorphism of the species (the two populations, *p between AB*) was estimated with one individual from each population (**Fig. S2**). Finally, the two GDI were compared to check if the Southern populations were more structured than the entire populations.

To contextualize these results, the same GDI measures were estimated for well-defined species of Carnivora. The species pairs used to make the comparison and thus help gauging the taxonomic status of the bat-eared fox and aardwolf subspecies were selected according to the following criteria: (1) the two species had to be as close as possible, (2) they had both reference genomes and short reads available, (3) their estimated coverage for the two species had to be greater than 20x, and (4) short read sequencing data had to be available for two individuals for one species of the pair. Given that, four species pairs were selected: (1) *Canis lupus* / *Canis aureus* (SRR8926747, SRR8926748, SRR7976426; vonHoldt et al.

2016); (2) *Ursus maritimus* / *Ursus arctos* (PB43: SRR942203, SRR942290, SRR942298; PB28: SRR942211, SRR942287, SRR942295; Brown Bear: SRR935591, SRR935625, SRR935627; Liu et al. 2014); (3) *Lynx pardinus* / *Lynx lynx* (Lynx pardinus LYNX11 : ERR1255591-ERR1255594; Lynx lynx LYNX8: ERR1255579-ERR1255582; Lynx lynx LYNX23: ERR1255540-ERR1255549; Abascal et al. 2016); and (4) *Panthera leo* / *Panthera pardus* (SRR10009886, SRR836361, SRR3041424; Kim et al. 2016). The exact same GDI estimation protocol was applied to each species pair.

Demographic analyses

Historical demographic variations in effective population size were estimated using the Pairwise Sequentially Markovian Coalescent (PSMC) model implemented in the software PSMC (https://github.com/lh3/psmc) (Li and Durbin, 2011). As described above, cleaned short reads were mapped against the corresponding reference genome using BWA-MEM (Li, 2013) and genotyping was performed using Freebayes v1.3.1-16 (git commit id: g85d7bfc) (Garrison and Marth, 2012) for the three individuals of each species. VCF files were converted to fasta format using a custom python script, excluding positions with quality below 20 and a depth of coverage below 10x or higher than 200x. Diploid sequences in fasta format were converted into PSMC fasta format using a C++ program written using the BIO++ library (Guéguen et al., 2013) with a block length of 100bp and excluding blocks containing more than 20% missing data as implemented in "fq2psmcfa" (https://github.com/lh3/psmc).

PSMC analyses were run for all other populations testing several -t and -p parameters including -p "4+30*2+4+6+10" (Nadachowska-Brzyska et al., 2013) and -p "4+25*2+4+6" (Kim et al., 2016) but also -p "4+10*3+4", -p "4+20*2+4" and -p "4+20*3+4". Overall, the tendencies were similar but some parameters led to unrealistic differences between the two

individuals from the South African population of *Otocyon megalotis*. We chose to present the results obtained using the parameters -t15 -r4 -p "4+10*3+4". For this parameter setting, the variance in ancestral effective population size was estimated by bootstrapping the scaffolds 100 times. To scale PSMC results, based on several previous studies on large mammals, a mutation rate of 10^{-8} mutation/site/generation (Ekblom et al., 2018; Gopalakrishnan et al., 2017) and a generation time of two years (Clark, 2005; Koehler and Richardson, 1990; van Jaarsveld, 1993) were selected. Results were plotted in R v3.63 (Team, 2020) using the function "psmc.results" (https://doi.org/10.5061/dryad.0618v/4) (Liu and Hansen, 2017) modifed using ggplot2 (Wickham, 2016) and cowplot (Wilke, 2016).

Phylogenomic inferences

To infer the Carnivora phylogenetic relationships, all carnivoran genomes available on Genbank, the DNAZoo website (https://www.dnazoo.org), and the OrthoMaM database (Scornavacca et al., 2019) as of February 11th, 2020 were downloaded (**Table S10**). In cases where more than one genome was available per species, the assembly with the best BUSCO scores was selected. Then, we annotated our two reference genome assemblies and the other unannotated assemblies using MAKER2 (Holt and Yandell, 2011) following the recommendations of the DNAZoo (https://www.dnazoo.org/post/the-first-million-genes-are-the-hardest-to-make-r). In the absence of available transcriptomic data, this method allowed to leverage the power of homology combined with the thorough knowledge accumulated on the gene content of mammalian genomes. As advised, a mammal-specific subset of UniProtKB/Swiss-Prot, a manually annotated, non-redundant protein sequence database, was used as a reference for this annotation step (Boutet et al., 2016). Finally, the annotated coding sequences (CDSs) recovered for the Southern aardwolf (*P. c. cristata*) were used to

assembled those of the Eastern aardwolf (*P. c. septentrionalis*) by mapping the resequenced Illumina reads using BWA-MEM (Li, 2013).

Orthologous genes were extracted following the orthology delineation process of the OrthoMaM database (OMM) (Scornavacca et al., 2019). First, for each orthologous gene alignment of OMM, a HMM profile was created via hmmbuild using default parameters of the HMMER toolkit (Eddy, 2011) and all HMM profiles were concatenated and summarized using hmmpress to construct a HMM database. Then, for each CDS newly annotated by MAKER, hmmscan was used on the HMM database to retrieve the best hits among the orthologous gene alignments. For each orthologous gene alignment, the most similar sequences for each species were detected via *hmmsearch*. Outputs from *hmmsearch* and *hmmscan* were discarded if the first hit score was not substantially better than the second ($hit_2 < 0.9\ hit_1$). This ensures our orthology predictions for the newly annotated CDSs to be robust. Then, the cleaning procedure of the OrthoMaM database was applied to the set of orthologous genes obtained. This process, implemented in a singularity image (Kurtzer et al., 2017) named *OMM_MACSE.sif* (Ranwez et al., 2020) is composed of several steps including nucleotide sequence alignment at the amino acid level with MAFFT (Katoh and Standley, 2013), refining alignments to handle frameshifts with MACSE v2 (Ranwez et al., 2018), cleaning of non homologous sequences, and masking of erroneous/dubious part of gene sequences with HMMcleaner (Di Franco et al., 2019). Finally, the last step of the cleaning process was to remove sequences that generated abnormally long branches during gene tree inferences. This was done by reconstructing gene trees using IQ-TREE v1.6.8 (Nguyen et al., 2014) with the MFP option to select the best fitting model for each gene. Then, the sequences generating abnormally long branches were identified and removed by *PhylteR* (https://github.com/damiendevienne/phylter). This software allows detecting and removing

928 outliers in phylogenomic datasets by iteratively removing taxa in genes and optimizing a
929 concordance score between individual distance matrices.

930 Phylogenomic analyses were performed using maximum likelihood (ML) using IQ-
931 TREE 1.6.8 (Nguyen et al., 2014) on the supermatrix resulting from the concatenation of all
932 orthologous genes previously recovered with the TESTNEW option to select the best fitting
933 model for each partition. Two partitions per gene were defined to separate the first two codon
934 positions from the third codon positions. Node supports were estimated with 100 non-
935 parametric bootstrap replicates. Furthermore, gene concordant (gCF) and site concordant
936 (sCF) factors were measured to complement traditional bootstrap node-support measures as
937 recommended in Minh et al. (Minh et al., 2020). For each orthologous gene alignment a gene
938 tree was inferred using IQ-TREE with a model selection and gCF and sCF were calculated
939 using the specific option -scf and -gcf in IQ-TREE (Minh et al., 2020). The gene trees
940 obtained with this analysis were also used to perform a coalescent-based species tree
941 inference using ASTRAL-III (Zhang et al., 2018).
942

943 ## Data access

944 Genome assemblies, associated SRA data and mitogenomes have been submited to genbank
945 and will be available after publication (XXXXXX-XXXXXX). The full analytical pipeline,
946 phylogenetic datasets (mitogenomic and genomic), corresponding trees and other
947 supplementary materials will be available from zenodo.org
948 (DOI:XX.XXXX/zenodo.XXXXXXX).

949 ## Disclosure declaration

950 The authors declare that they have no competing interests.

Funding

This work was supported by grants from the European Research Council (ERC-2015-CoG-683257 ConvergeAnt project), Investissements d'Avenir of the Agence Nationale de la Recherche (CEMEB: ANR-10-LABX-0004; ReNaBi-IFB: ANR-11-INBS-0013; MGX: ANR-10-INBS-09).

Acknowledgements

We would like to thank Rachid Koual and Amandine Magdeleine for technical help with DNA extractions and library preprations, Aude Caizergues and Nathalie Delsuc for fieldwork assistance, Christian Fontaine, Jean-Christophe Vié (Faune Sauvage, French Guiana), Corine Esser (Fauverie du Mont Faron, Toulon, France), François Catzeflis (ISEM Mammalian Tissue Collection), Adam Ferguson and Bruce Patterson (Field Museum of Natural History, Chicago, USA), Lily Crowley (Hamerton Zoo Park, UK), and Andrew Kitchener (National Museum of Scotland, Edinburgh, UK) for access to tissue samples. We also acknowledge Pierre-Alexandre Gagnaire for helpful discussion on genetic differentiation index and Brian Chase for providing references on African paleoclimate. We thank the Montpellier GenomiX Plateform (MGX) part of the France Génomique National Infrastructure for sequencing data generation. Computational analyses benefited from the Montpellier Bioinformatics Biodiversity platform. We are also grateful to the Institut Français de Bioinformatique and the Roscoff Bioinformatics platform ABiMS (http://abims.sb-roscoff.fr) for providing help for computing and storage resources. This is contribution ISEM 2020-XXX-SUD of the Institut des Sciences de l'Evolution de Montpellier.

Authors' contributions

RA, BN and FD conceived the ideas and designed methodology, analysed the data, and led the writing of the manuscript; FD, NLA and RA performed fieldwork sampling; MK, RA and FD developed the protocol and performed DNA long-read sequencing; MK performed molecular biology experiments; RA, CS, EC and BN performed the bioinformatic analyses; FD and EC provided access to computational resources. All authors contributed critically to the drafts and gave final approval for publication.

References

200 mammals project. n.d. Comparative Genomics – 200 Mammals.

Abascal F, Corvelo A, Cruz F, Villanueva-Cañas JL, Vlasova A, Marcet-Houben M, Martínez-Cruz B, Cheng JY, Prieto P, Quesada V, Quilez J, Li G, García F, Rubio-Camarillo M, Frias L, Ribeca P, Capella-Gutiérrez S, Rodríguez JM, Câmara F, Lowy E, Cozzuto L, Erb I, Tress ML, Rodriguez-Ales JL, Ruiz-Orera J, Reverter F, Casas-Marce M, Soriano L, Arango JR, Derdak S, Galán B, Blanc J, Gut M, Lorente-Galdos B, Andrés-Nieto M, López-Otín C, Valencia A, Gut I, García JL, Guigó R, Murphy WJ, Ruiz-Herrera A, Marques-Bonet T, Roma G, Notredame C, Mailund T, Albà MM, Gabaldón T, Alioto T, Godoy JA. 2016. Extreme genomic erosion after recurrent demographic bottlenecks in the highly endangered Iberian lynx. *Genome Biol* **17**:251. doi:10.1186/s13059-016-1090-1

Agnarsson I, Kuntner M, May-Collado LJ. 2010. Dogs, cats, and kin: A molecular species-level phylogeny of Carnivora. *Mol Phylogenet Evol* **54**:726–745. doi:10.1016/J.YMPEV.2009.10.033

Aird D, Ross MG, Chen WS, Danielsson M, Fennell T, Russ C, Jaffe DB, Nusbaum C, Gnirke A. 2011. Analyzing and minimizing PCR amplification bias in Illumina sequencing libraries. *Genome Biol* **12**:R18. doi:10.1186/gb-2011-12-2-r18

Allen R, Ryan H, Davis BW, King C, Frantz L, Irving-Pease E, Barnett R, Linderholm A, Loog L, Haile J, Lebrasseur O, White M, Kitchener AC, Murphy WJ, Larson G. 2020. A mitochondrial genetic divergence proxy predicts the reproductive compatibility of mammalian hybrids. *Proc R Soc B Biol Sci* **287**:20200690. doi:10.1098/rspb.2020.0690

Allio R, Schomaker-Bastos A, Romiguier J, Prosdocimi F, Nabholz B, Delsuc F. 2020a. MitoFinder: Efficient automated large-scale extraction of mitogenomic data in target enrichment phylogenomics. *Mol Ecol Resour* 1755–0998.13160. doi:10.1111/1755-0998.13160

Allio R, Scornavacca C, Nabholz B, Clamens A-L, Sperling FA, Condamine FL. 2020b. Whole genome shotgun phylogenomics resolves the pattern and timing of swallowtail butterfly evolution. *Syst Biol* **69**:38–60. doi:10.1093/sysbio/syz030

Armstrong EE, Taylor RW, Miller DE, Kaelin CB, Barsh GS, Hadly EA, Petrov D. 2020.

1010 Long live the king: chromosome-level assembly of the lion (Panthera leo) using linked-
1011 read, Hi-C, and long-read data. *BMC Biol* **18**:3. doi:10.1186/s12915-019-0734-5

1012 Arnason U, Gullberg A, Janke A, Kullberg M. 2007. Mitogenomic analyses of caniform
1013 relationships. *Mol Phylogenet Evol* **45**:863–874. doi:10.1016/J.YMPEV.2007.06.019

1014 Atickem A, Stenseth NC, Drouilly M, Bock S, Roos C, Zinner D. 2018. Deep divergence
1015 among mitochondrial lineages in African jackals. *Zool Scr* **47**:1–8.
1016 doi:10.1111/zsc.12257

1017 Barnett R, Yamaguchi N, Barnes I, Cooper A. 2006. The origin, current diversity and future
1018 conservation of the modern lion (*Panthera leo*). *Proc R Soc B Biol Sci* **273**:2119–2125.
1019 doi:10.1098/rspb.2006.3555

1020 Batra SS, Levy-Sakin M, Robinson J, Guillory J, Durinck S, Kwok P-Y, Cox LA, Seshagiri
1021 S, Song YS, Wall JD. 2019a. Accurate assembly of the olive baboon (*Papio anubis*)
1022 genome using long--read and Hi-C data. *bioRxiv* 678771. doi:10.1101/678771

1023 Batra SS, Levy-Sakin M, Robinson J, Guillory J, Durinck S, Kwok P-Y, Cox LA, Seshagiri
1024 S, Song YS, Wall JD. 2019b. Accurate assembly of the olive baboon (Papio anubis)
1025 genome using long--read and Hi-C data. *bioRxiv* 678771. doi:10.1101/678771

1026 Blaimer BB, LaPolla JS, Branstetter MG, Lloyd MW, Brady SG. 2016. Phylogenomics,
1027 biogeography and diversification of obligate mealybug-tending ants in the genus
1028 Acropyga. *Mol Phylogenet Evol* **102**:20–29. doi:10.1016/J.YMPEV.2016.05.030

1029 Blanco MB, Greene LK, Williams RC, Andrianandrasana L, Yoder AD, Larsen PA. 2019.
1030 Next-generation in situ conservation and educational outreach in Madagascar using a
1031 mobile genetics lab. *bioRxiv* 650614. doi:10.1101/650614

1032 Bolger AM, Lohse M, Usadel B. 2014. Trimmomatic: A flexible trimmer for Illumina
1033 sequence data. *Bioinformatics* **30**:2114–2120. doi:10.1093/bioinformatics/btu170

1034 Boutet E, Lieberherr D, Tognolli M, Schneider M, Bansal P, Bridge AJ, Poux S, Bougueleret
1035 L, Xenarios I. 2016. UniProtKB/Swiss-Prot, the manually annotated section of the
1036 UniProt KnowledgeBase: How to use the entry view. Humana Press, New York, NY.
1037 pp. 23–54. doi:10.1007/978-1-4939-3167-5_2

1038 Caley T, Extier T, Collins JA, Schefuß E, Dupont L, Malaizé B, Rossignol L, Souron A,
1039 McClymont EL, Jimenez-Espejo FJ, García-Comas C, Eynaud F, Martinez P, Roche
1040 DM, Jorry SJ, Charlier K, Wary M, Gourves PY, Billy I, Giraudeau J. 2018. A two-
1041 million-year-long hydroclimatic context for hominin evolution in southeastern Africa.
1042 *Nature* **560**:76–79. doi:10.1038/s41586-018-0309-6

1043 Casas-Marce M, Soriano L, López-Bao J V., Godoy JA. 2013. Genetics at the verge of
1044 extinction: insights from the Iberian lynx. *Mol Ecol* **22**:5503–5515.
1045 doi:10.1111/mec.12498

1046 Chase BM, Niedermeyer EM, Boom A, Carr AS, Chevalier M, He F, Meadows ME, Ogle N,
1047 Reimer PJ. 2019. Orbital controls on Namib Desert hydroclimate over the past 50,000
1048 years. *Geology* **47**:867–871. doi:10.1130/G46334.1

1049 Chevalier M, Chase BM. 2015. Southeast African records reveal a coherent shift from high-
1050 to low-latitude forcing mechanisms along the east African margin across last glacial-
1051 interglacial transition. *Quat Sci Rev* **125**:117–130. doi:10.1016/j.quascirev.2015.07.009

1052 Clark HO. 2005. Otocyon megalotis. *Mamm Species* 1–5. doi:10.1644/1545-
1053 1410(2005)766[0001:OM]2.0.CO;2

1054 Datema E, Hulzink RJM, Blommers L, Valle-Inclan JE, Orsouw N van, Wittenberg AHJ,
1055 Vos M de. 2016. The megabase-sized fungal genome of Rhizoctonia solani assembled
1056 from nanopore reads only. *bioRxiv* 084772. doi:10.1101/084772

1057 De Queiroz K. 2007. Species concepts and species delimitation. *Syst Biol* **56**:879–886.
1058 doi:10.1080/10635150701701083

1059 Dehghani R, Wanntorp L, Pagani P, Källersjö M, Werdelin L, Veron G. 2008.
1060 Phylogeography of the white-tailed mongoose (Herpestidae, Carnivora, Mammalia)
1061 based on partial sequences of the mtDNA control region. *J Zool* **276**:385–393.
1062 doi:10.1111/j.1469-7998.2008.00502.x

1063 Delisle I, Strobeck C. 2005. A phylogeny of the Caniformia (order Carnivora) based on 12
1064 complete protein-coding mitochondrial genes. *Mol Phylogenet Evol* **37**:192–201.
1065 doi:10.1016/J.YMPEV.2005.04.025

1066 deMenocal PB. 2004. African climate change and faunal evolution during the Pliocene-
1067 Pleistocene. *Earth Planet Sci Lett* **220**:3–24. doi:10.1016/S0012-821X(04)00003-2

1068 deMenocal PB. 1995. Plio-Pleistocene African climate. *Science (80-)*.
1069 doi:10.1126/science.270.5233.53

1070 Di Genova A, Ruz GA, Sagot M-F, Maass A. 2018. Fast-SG: an alignment-free algorithm for
1071 hybrid assembly. *Gigascience* **7**. doi:10.1093/gigascience/giy048

1072 Di Franco A, Poujol R, Baurain D, Philippe H. 2019. Evaluating the usefulness of alignment
1073 filtering methods to reduce the impact of errors on evolutionary inferences. *BMC Evol*
1074 *Biol* **19**:21. doi:10.1186/s12862-019-1350-2

1075 Díaz-Viraqué F, Pita S, Greif G, de Souza R de CM, Iraola G, Robello C. 2019. Nanopore
1076 sequencing significantly improves genome assembly of the protozoan parasite
1077 *Trypanosoma cruzi*. *Genome Biol Evol* **11**:1952–1957. doi:10.1093/gbe/evz129

1078 DISCOVAR | Assemble genomes, find variants. n.d.
1079 https://software.broadinstitute.org/software/discovar/blog/

1080 Doronina L, Churakov G, Shi J, Brosius J, Baertsch R, Clawson H, Schmitz J. 2015.
1081 Exploring massive incomplete lineage sorting in Arctoids (Laurasiatheria, Carnivora).
1082 *Mol Biol Evol* **32**:msv188. doi:10.1093/molbev/msv188

1083 Dudchenko O, Batra SS, Omer AD, Nyquist SK, Hoeger M, Durand NC, Shamim MS,
1084 Machol I, Lander ES, Aiden AP, Aiden EL. 2017. De novo assembly of the Aedes
1085 aegypti genome using Hi-C yields chromosome-length scaffolds. *Science (80-)* **356**:92–
1086 95. doi:10.1126/science.aal3327

1087 Eddy SR. 2011. Accelerated profile HMM searches. *PLoS Comput Biol* **7**.
1088 doi:10.1371/journal.pcbi.1002195

1089 Eizirik E, Murphy WJ, Koepfli K-P, Johnson WE, Dragoo JW, Wayne RK, O'Brien SJ.
1090 2010. Pattern and timing of diversification of the mammalian order Carnivora inferred
1091 from multiple nuclear gene sequences. *Mol Phylogenet Evol* **56**:49–63.
1092 doi:10.1016/J.YMPEV.2010.01.033

1093 Ekblom R, Brechlin B, Persson J, Smeds L, Johansson M, Magnusson J, Flagstad Ø, Ellegren
1094 H. 2018. Genome sequencing and conservation genomics in the Scandinavian wolverine
1095 population. *Conserv Biol* **32**:1301–1312. doi:10.1111/cobi.13157

1096 Etherington GJ, Heavens D, Baker D, Lister A, McNelly R, Garcia G, Clavijo B, Macaulay I,
1097 Haerty W, Di Palma F. 2020. Sequencing smart: *De novo* sequencing and assembly
1098 approaches for a non-model mammal. *Gigascience* **9**.
1099 doi:10.1093/GIGASCIENCE/GIAA045

1100 Faurby S, Eiserhardt WL, Svenning J. 2016. Strong effects of variation in taxonomic opinion
1101 on diversification analyses. *Methods Ecol Evol* **7**:4–13. doi:10.1111/2041-210X.12449

1102 Flynn JJ, Finarelli JA, Spaulding M. 2010. Phylogeny of the Carnivora and
1103 Carnivoramorpha, and the use of the fossil record to enhance understanding of
1104 evolutionary transformations In: Goswami A, Friscia A, editors. Carnivoran Evolution.
1105 Cambridge: Cambridge University Press. pp. 25–63.
1106 doi:10.1017/CBO9781139193436.003

1107 Flynn JJ, Finarelli JA, Zehr S, Hsu J, Nedbal MA. 2005. Molecular phylogeny of the
1108 Carnivora (Mammalia): assessing the impact of increased sampling on resolving
1109 enigmatic relationships. *Syst Biol* **54**:317–337. doi:10.1080/10635150590923326

1110 Flynn JJ, Nedbal MA. 1998. Phylogeny of the Carnivora (Mammalia): congruence vs
1111 incompatibility among multiple data sets. *Mol Phylogenet Evol* **9**:414–426.
1112 doi:10.1006/MPEV.1998.0504

1113 Frankham R, Ballou JD, Dudash MR, Eldridge MDB, Fenster CB, Lacy RC, Mendelson JR,
1114 Porton IJ, Ralls K, Ryder OA. 2012. Implications of different species concepts for
1115 conserving biodiversity. *Biol Conserv* **153**:25–31. doi:10.1016/J.BIOCON.2012.04.034

1116 Galov A, Fabbri E, Caniglia R, Arbanasić H, Lapalombella S, Florijančić T, Bošković I,
1117 Galaverni M, Randi E. 2015. First evidence of hybridization between golden jackal (
1118 *Canis aureus*) and domestic dog (*Canis familiaris*) as revealed by genetic markers. *R*
1119 *Soc Open Sci* **2**:150450. doi:10.1098/rsos.150450

1120 Galtier N. 2019. Delineating species in the speciation continuum: A proposal. *Evol Appl*
1121 **12**:657–663. doi:10.1111/eva.12748

1122 Galtier N, Nabholz B, Glémin S, Hurst GDD. 2009. Mitochondrial DNA as a marker of
1123 molecular diversity: a reappraisal. *Mol Ecol* **18**:4541–4550. doi:10.1111/j.1365-
1124 294X.2009.04380.x

1125 Gan HM, Falk S, Morales HE, Austin CM, Sunnucks P, Pavlova A. 2019. Genomic evidence
1126 of neo-sex chromosomes in the eastern yellow robin. *Gigascience* **8**.
1127 doi:10.1093/gigascience/giz111

1128 Garrison E, Marth G. 2012. Haplotype-based variant detection from short-read sequencing.

1129 Gopalakrishnan S, Samaniego Castruita JA, Sinding M-HS, Kuderna LFK, Räikkönen J,
1130 Petersen B, Sicheritz-Ponten T, Larson G, Orlando L, Marques-Bonet T, Hansen AJ,
1131 Dalén L, Gilbert MTP. 2017. The wolf reference genome sequence (Canis lupus lupus)
1132 and its implications for Canis spp. population genomics. *BMC Genomics* **18**:495.
1133 doi:10.1186/s12864-017-3883-3

1134 Gopalakrishnan S, Sinding M-HS, Ramos-Madrigal J, Niemann J, Samaniego Castruita JA,

1135 Vieira FG, Carøe C, Montero M de M, Kuderna L, Serres A, González-Basallote VM,
1136 Liu Y-H, Wang G-D, Marques-Bonet T, Mirarab S, Fernandes C, Gaubert P, Koepfli K-
1137 P, Budd J, Rueness EK, Sillero C, Heide-Jørgensen MP, Petersen B, Sicheritz-Ponten T,
1138 Bachmann L, Wiig Ø, Hansen AJ, Gilbert MTP. 2018. Interspecific gene flow shaped
1139 the evolution of the genus Canis. *Curr Biol* **28**:3441–3449.e5.
1140 doi:10.1016/J.CUB.2018.08.041

1141 Grant KM, Rohling EJ, Westerhold T, Zabel M, Heslop D, Konijnendijk T, Lourens L. 2017.
1142 A 3 million year index for North African humidity/aridity and the implication of
1143 potential pan-African Humid periods. *Quat Sci Rev* **171**:100–118.
1144 doi:10.1016/j.quascirev.2017.07.005

1145 Guéguen L, Gaillard S, Boussau B, Gouy M, Groussin M, Rochette NC, Bigot T, Fournier D,
1146 Pouyet F, Cahais V, Bernard A, Scornavacca C, Nabholz B, Haudry A, Dachary L,
1147 Galtier N, Belkhir K, Dutheil JY. 2013. Bio++: Efficient extensible libraries and tools
1148 for computational molecular evolution. *Mol Biol Evol* **30**:1745–1750.
1149 doi:10.1093/molbev/mst097

1150 Guschanski K, Krause J, Sawyer S, Valente LM, Bailey S, Finstermeier K, Sabin R, Gilissen
1151 E, Sonet G, Nagy ZT, Lenglet G, Mayer F, Savolainen V. 2013. Next-generation
1152 museomics disentangles one of the largest primate radiations. *Syst Biol* **62**:539–554.
1153 doi:10.1093/sysbio/syt018

1154 Holsinger KE, Weir BS. 2009. Genetics in geographically structured populations: defining,
1155 estimating and interpreting FST. *Nat Rev Genet* **10**:639–650. doi:10.1038/nrg2611

1156 Holt C, Yandell M. 2011. MAKER2: an annotation pipeline and genome-database
1157 management tool for second-generation genome projects. *BMC Bioinformatics* **12**:491.
1158 doi:10.1186/1471-2105-12-491

1159 Hudson RR, Slatkin M, Maddison WP. 1992. Estimation of levels of gene flow from DNA
1160 sequence data. *Genetics* **132**.

1161 IUCN 2020. 2020. The IUCN Red List of Threatened Species. Version 2020-1.
1162 https://www.iucnredlist.org.

1163 Jain M, Koren S, Miga KH, Quick J, Rand AC, Sasani TA, Tyson JR, Beggs AD, Dilthey
1164 AT, Fiddes IT, Malla S, Marriott H, Nieto T, O'Grady J, Olsen HE, Pedersen BS, Rhie
1165 A, Richardson H, Quinlan AR, Snutch TP, Tee L, Paten B, Phillippy AM, Simpson JT,
1166 Loman NJ, Loose M. 2018. Nanopore sequencing and assembly of a human genome
1167 with ultra-long reads. *Nat Biotechnol* **36**:338–345. doi:10.1038/nbt.4060

1168 Jain M, Olsen HE, Paten B, Akeson M. 2016. The Oxford Nanopore MinION: delivery of
1169 nanopore sequencing to the genomics community. *Genome Biol* **17**:239.
1170 doi:10.1186/s13059-016-1103-0

1171 Jansen HJ, Liem M, Jong-Raadsen SA, Dufour S, Weltzien F-A, Swinkels W, Koelewijn A,
1172 Palstra AP, Pelster B, Spaink HP, Thillart GE van den, Dirks RP, Henkel C V. 2017.
1173 Rapid de novo assembly of the European eel genome from nanopore sequencing reads.
1174 *Sci Rep* **7**:7213. doi:10.1038/s41598-017-07650-6

1175 Jeffroy O, Brinkmann H, Delsuc F, Philippe H. 2006. Phylogenomics: the beginning of
1176 incongruence? *Trends Genet* **22**:225–231. doi:10.1016/J.TIG.2006.02.003

1177 Jiang JB, Quattrini AM, Francis WR, Ryan JF, Rodríguez E, McFadden CS. 2019. A hybrid
1178 de novo assembly of the sea pansy (Renilla muelleri) genome. *Gigascience* **8**.
1179 doi:10.1093/gigascience/giz026

1180 Johnson TC, Werne JP, Brown ET, Abbott A, Berke M, Steinman BA, Halbur J, Contreras S,
1181 Grosshuesch S, Deino A, Scholz CA, Lyons RP, Schouten S, Damsté JSS. 2016. A
1182 progressively wetter climate in southern East Africa over the past 1.3 million years.
1183 *Nature* **537**:220–224. doi:10.1038/nature19065

1184 Kadobianskyi M, Schulze L, Schuelke M, Judkewitz B. 2019. Hybrid genome assembly and
1185 annotation of Danionella translucida, a transparent fish with the smallest known
1186 vertebrate brain. *bioRxiv* 539692. doi:10.1101/539692

1187 Kalyaanamoorthy S, Minh BQ, Wong TKF, von Haeseler A, Jermiin LS. 2017. ModelFinder:
1188 fast model selection for accurate phylogenetic estimates. *Nat Methods* **14**:587–589.
1189 doi:10.1038/nmeth.4285

1190 Katoh K, Standley DM. 2013. MAFFT multiple sequence alignment oftware version 7:
1191 Improvements in performance and usability. *Mol Biol Evol* **30**:772–780.
1192 doi:10.1093/molbev/mst010

1193 Kearse M, Moir R, Wilson A, Stones-Havas S, Cheung M, Sturrock S, Buxton S, Cooper A,
1194 Markowitz S, Duran C, Thierer T, Ashton B, Meintjes P, Drummond A. 2012. Geneious
1195 Basic: An integrated and extendable desktop software platform for the organization and
1196 analysis of sequence data. *Bioinformatics* **28**:1647–1649.
1197 doi:10.1093/bioinformatics/bts199

1198 Kim S, Cho YS, Kim H-M, Chung O, Kim H, Jho S, Seomun H, Kim J, Bang WY, Kim C,
1199 An J, Bae CH, Bhak Y, Jeon S, Yoon H, Kim Y, Jun J, Lee H, Cho S, Uphyrkina O,
1200 Kostyria A, Goodrich J, Miquelle D, Roelke M, Lewis J, Yurchenko A, Bankevich A,
1201 Cho J, Lee S, Edwards JS, Weber JA, Cook J, Kim S, Lee H, Manica A, Lee I, O'Brien
1202 SJ, Bhak J, Yeo J-H. 2016. Comparison of carnivore, omnivore, and herbivore
1203 mammalian genomes with a new leopard assembly. *Genome Biol* **17**:211.
1204 doi:10.1186/s13059-016-1071-4

1205 Koehler CE, Richardson PRK. 1990. Proteles cristatus. *Mamm Species* 1–6.
1206 doi:10.2307/3504197

1207 Koepfli K-P, Jenks SM, Eizirik E, Zahirpour T, Valkenburgh B Van, Wayne RK. 2006.
1208 Molecular systematics of the Hyaenidae: Relationships of a relictual lineage resolved by
1209 a molecular supermatrix. *Mol Phylogenet Evol* **38**:603–620.
1210 doi:10.1016/J.YMPEV.2005.10.017

1211 Koepfli K-P, Paten B, O'Brien SJ. 2015. The Genome 10K Project: A Way Forward. *Annu*
1212 *Rev Anim Biosci* **3**:57–111. doi:10.1146/annurev-animal-090414-014900

1213 Koren S, Walenz BP, Berlin K, Miller JR, Bergman NH, Phillippy AM. 2017. Canu: scalable
1214 and accurate long-read assembly via adaptive k-mer weighting and repeat separation.
1215 *Genome Res* **27**:722–736. doi:10.1101/GR.215087.116

1216 Kumar S, Filipski AJ, Battistuzzi FU, Kosakovsky Pond SL, Tamura K. 2012. Statistics and
1217 truth in phylogenomics. *Mol Biol Evol* **29**:457–472. doi:10.1093/molbev/msr202

1218 Kurtzer GM, Sochat V, Bauer MW. 2017. Singularity: Scientific containers for mobility of

compute. *PLoS One* **12**:e0177459. doi:10.1371/journal.pone.0177459

Kwan HH, Culibrk L, Taylor GA, Leelakumari S, Tan R, Jackman SD, Tse K, MacLeod T, Cheng D, Chuah E, Kirk H, Pandoh P, Carlsen R, Zhao Y, Mungall AJ, Moore R, Birol I, Marra MA, Rosen DAS, Haulena M, Jones SJM, Kwan HH, Culibrk L, Taylor GA, Leelakumari S, Tan R, Jackman SD, Tse K, MacLeod T, Cheng D, Chuah E, Kirk H, Pandoh P, Carlsen R, Zhao Y, Mungall AJ, Moore R, Birol I, Marra MA, Rosen DAS, Haulena M, Jones SJM. 2019. The Genome of the Steller Sea Lion (Eumetopias jubatus). *Genes (Basel)* **10**:486. doi:10.3390/genes10070486

L Y, YP Z. 2006. Phylogeny of the caniform Carnivora: evidence from multiple genes. *Genetica* **127**. doi:10.1007/S10709-005-2482-4

Laetsch DR, Blaxter ML. 2017. BlobTools: Interrogation of genome assemblies. *F1000Research* **6**:1287. doi:10.12688/f1000research.12232.1

Lartillot N, Rodrigue N, Stubbs D, Richer J. 2013. PhyloBayes MPI: Phylogenetic reconstruction with infinite mixtures of profiles in a parallel environment. *Syst Biol* **62**:611–615. doi:10.1093/sysbio/syt022

Li G, Davis BW, Eizirik E, Murphy WJ. 2016. Phylogenomic evidence for ancient hybridization in the genomes of living cats (Felidae). *Genome Res* **26**:1–11. doi:10.1101/GR.186668.114

Li H. 2013. Aligning sequence reads, clone sequences and assembly contigs with BWA-MEM.

Li H, Durbin R. 2011. Inference of human population history from individual whole-genome sequences. *Nature* **475**:493–496. doi:10.1038/nature10231

Li H, Handsaker B, Wysoker A, Fennell T, Ruan J, Homer N, Marth G, Abecasis G, Durbin R. 2009. The sequence alignment/map format and SAMtools. *Bioinformatics* **25**:2078–2079. doi:10.1093/bioinformatics/btp352

Li R, Fan W, Tian G, Zhu H, He L, Cai J, Huang Q, Cai Q, Li B, Bai Y, Zhang Z, Zhang Y, Wang W, Li J, Wei F, Li H, Jian M, Li J, Zhang Z, Nielsen R, Li D, Gu W, Yang Z, Xuan Z, Ryder OA, Leung FCC, Zhou Y, Cao J, Sun X, Fu Y, Fang X, Guo X, Wang B, Hou R, Shen F, Mu B, Ni P, Lin R, Qian W, Wang G, Yu C, Nie W, Wang J, Wu Z, Liang H, Min J, Wu Q, Cheng S, Ruan J, Wang M, Shi Z, Wen M, Liu B, Ren X, Zheng H, Dong D, Cook K, Shan G, Zhang H, Kosiol C, Xie X, Lu Z, Zheng H, Li Y, Steiner CC, Lam TTY, Lin S, Zhang Q, Li G, Tian J, Gong T, Liu H, Zhang D, Fang L, Ye C, Zhang J, Hu W, Xu A, Ren Y, Zhang G, Bruford MW, Li Q, Ma L, Guo Y, An N, Hu Y, Zheng Y, Shi Y, Li Z, Liu Q, Chen Y, Zhao J, Qu N, Zhao S, Tian F, Wang X, Wang H, Xu L, Liu X, Vinar T, Wang Y, Lam TW, Yiu SM, Liu S, Zhang H, Li D, Huang Y, Wang X, Yang G, Jiang Z, Wang J, Qin N, Li L, Li J, Bolund L, Kristiansen K, Wong GKS, Olson M, Zhang X, Li S, Yang H, Wang J, Wang J. 2010. The sequence and de novo assembly of the giant panda genome. *Nature* **463**:311–317. doi:10.1038/nature08696

Lim S, Chase BM, Chevalier M, Reimer PJ. 2016. 50,000 years of vegetation and climate change in the southern Namib Desert, Pella, South Africa. *Palaeogeogr Palaeoclimatol Palaeoecol* **451**:197–209. doi:10.1016/j.palaeo.2016.03.001

Lindblad-Toh K, Garber M, Zuk O, Lin MF, Parker BJ, Washietl S, Kheradpour P, Ernst J,

Jordan G, Mauceli E, Ward LD, Lowe CB, Holloway AK, Clamp M, Gnerre S, Alföldi J, Beal K, Chang J, Clawson H, Cuff J, Di Palma F, Fitzgerald S, Flicek P, Guttman M, Hubisz MJ, Jaffe DB, Jungreis I, Kent WJ, Kostka D, Lara M, Martins AL, Massingham T, Moltke I, Raney BJ, Rasmussen MD, Robinson J, Stark A, Vilella AJ, Wen J, Xie X, Zody MC, Worley KC, Kovar CL, Muzny DM, Gibbs RA, Warren WC, Mardis ER, Weinstock GM, Wilson RK, Birney E, Margulies EH, Herrero J, Green ED, Haussler D, Siepel A, Goldman N, Pollard KS, Pedersen JS, Lander ES, Kellis M, Baldwin J, Bloom T, Chin CW, Heiman D, Nicol R, Nusbaum C, Young S, Wilkinson J, Cree A, Dihn HH, Fowler G, Jhangiani S, Joshi V, Lee S, Lewis LR, Nazareth L V., Okwuonu G, Santibanez J, Delehaunty K, Dooling D, Fronik C, Fulton L, Fulton B, Graves T, Minx P, Sodergren E. 2011. A high-resolution map of human evolutionary constraint using 29 mammals. *Nature* **478**:476–482. doi:10.1038/nature10530

Liu S, Hansen MM. 2017. PSMC (pairwise sequentially Markovian coalescent) analysis of RAD (restriction site associated DNA) sequencing data. *Mol Ecol Resour* **17**:631–641. doi:10.1111/1755-0998.12606

Liu S, Lorenzen ED, Fumagalli M, Li B, Harris K, Xiong Z, Zhou L, Korneliussen TS, Somel M, Babbitt C, Wray G, Li J, He W, Wang Z, Fu W, Xiang X, Morgan CC, Doherty A, O'Connell MJ, McInerney JO, Born EW, Dalén L, Dietz R, Orlando L, Sonne C, Zhang G, Nielsen R, Willerslev E, Wang J. 2014. Population genomics reveal recent speciation and rapid evolutionary adaptation in polar bears. *Cell* **157**:785–794. doi:10.1016/J.CELL.2014.03.054

Lorenzen ED, Heller R, Siegismund HR. 2012. Comparative phylogeography of African savannah ungulates 1. *Mol Ecol* **21**:3656–3670. doi:10.1111/j.1365-294X.2012.05650.x

Luo R, Liu B, Xie Y, Li Z, Huang W, Yuan J, He G, Chen Y, Pan Q, Liu Y, Tang J, Wu G, Zhang H, Shi Y, Liu Y, Yu C, Wang B, Lu Y, Han C, Cheung DW, Yiu S-M, Peng S, Xiaoqian Z, Liu G, Liao X, Li Y, Yang H, Wang J, Lam T-W, Wang J. 2012. SOAPdenovo2: An empirically improved memory-efficient short-read de novo assembler. *Gigascience* **1**:18. doi:10.1186/2047-217X-1-18

Maigret TA. 2019. Snake scale clips as a source of high quality DNA suitable for RAD sequencing. *Conserv Genet Resour* **11**:373–375. doi:10.1007/s12686-018-1019-y

Maslin MA, Brierley CM, Milner AM, Shultz S, Trauth MH, Wilson KE. 2014. East african climate pulses and early human evolution. *Quat Sci Rev*. doi:10.1016/j.quascirev.2014.06.012

Meredith RW, Janečka JE, Gatesy J, Ryder OA, Fisher CA, Teeling EC, Goodbla A, Eizirik E, Simão TLL, Stadler T, Rabosky DL, Honeycutt RL, Flynn JJ, Ingram CM, Steiner C, Williams TL, Robinson TJ, Burk-Herrick A, Westerman M, Ayoub NA, Springer MS, Murphy WJ. 2011. Impacts of the cretaceous terrestrial revolution and KPg extinction on mammal diversification. *Science (80-)* **334**:521–524. doi:10.1126/SCIENCE.1211028

Meyer CP, Paulay G. 2005. DNA barcoding: error rates based on comprehensive sampling. *PLoS Biol* **3**:e422. doi:10.1371/journal.pbio.0030422

Michael TP, Jupe F, Bemm F, Motley ST, Sandoval JP, Lanz C, Loudet O, Weigel D, Ecker JR. 2018. High contiguity Arabidopsis thaliana genome assembly with a single nanopore flow cell. *Nat Commun* **9**:541. doi:10.1038/s41467-018-03016-2

Miller JM, Hallager S, Monfort SL, Newby J, Bishop K, Tidmus SA, Black P, Houston B, Matthee CA, Fleischer RC, Hallager S, Monfort SL, Newby J, Bishop ÁK, Tidmus SA, Black P, Houston ÁB, Matthee CA. 2011. Phylogeographic analysis of nuclear and mtDNA supports subspecies designations in the ostrich (Struthio camelus). *Conserv Genet* **12**:423–431. doi:10.1007/s10592-010-0149-x

Minh BQ, Hahn MW, Lanfear R. 2020. New methods to calculate concordance factors for phylogenomic datasets. *Mol Biol Evol*. doi:10.1093/molbev/msaa106

Nadachowska-Brzyska K, Burri R, Olason PI, Kawakami T, Smeds L, Ellegren H. 2013. Demographic divergence history of pied flycatcher and collared flycatcher inferred from whole-genome re-sequencing data. *PLoS Genet* **9**:e1003942. doi:10.1371/journal.pgen.1003942

Nguyen L-T, Schmidt HA, von Haeseler A, Minh BQ. 2014. IQ-TREE: A fast and effective stochastic algorithm for estimating maximum-likelihood phylogenies. *Mol Biol Evol* **32**:268–274. doi:10.1093/molbev/msu300

Nicholls SM, Quick JC, Tang S, Loman NJ. 2019. Ultra-deep, long-read nanopore sequencing of mock microbial community standards. *Gigascience* **8**. doi:10.1093/gigascience/giz043

Nishimura O, Hara Y, Kuraku S. 2017. gVolante for standardizing completeness assessment of genome and transcriptome assemblies. *Bioinformatics* **33**:3635–3637. doi:10.1093/bioinformatics/btx445

Parker J, Helmstetter AJ, Devey D, Wilkinson T, Papadopulos AST. 2017. Field-based species identification of closely-related plants using real-time nanopore sequencing. *Sci Rep* **7**:8345. doi:10.1038/s41598-017-08461-5

Peng R, Zeng B, Meng X, Yue B, Zhang Z, Zou F. 2007. The complete mitochondrial genome and phylogenetic analysis of the giant panda (Ailuropoda melanoleuca). *Gene* **397**:76–83. doi:10.1016/J.GENE.2007.04.009

Périquet S, Roxburgh L, le Roux A, Collinson WJ. 2018. Testing the value of citizen science for roadkill studies: A case study from South Africa. *Front Ecol Evol* **6**:15. doi:10.3389/fevo.2018.00015

Pomerantz A, Peñafiel N, Arteaga A, Bustamante L, Pichardo F, Coloma LA, Barrio-Amorós CL, Salazar-Valenzuela D, Prost S. 2018. Real-time DNA barcoding in a rainforest using nanopore sequencing: opportunities for rapid biodiversity assessments and local capacity building. *Gigascience* **7**. doi:10.1093/gigascience/giy033

Ranwez V, Chantret N, Delsuc F. 2020. Aligning protein-coding nucleotide sequences with MACSE. *Methods Mol Biol* **In press**.

Ranwez V, Douzery EJP, Cambon C, Chantret N, Delsuc F. 2018. MACSE v2: Toolkit for the alignment of coding sequences accounting for frameshifts and stop codons. *Mol Biol Evol* **35**:2582–2584. doi:10.1093/molbev/msy159

Ravinet M, Westram A, Johannesson K, Butlin R, André C, Panova M. 2016. Shared and nonshared genomic divergence in parallel ecotypes of *Littorina saxatilis* at a local scale. *Mol Ecol* **25**:287–305. doi:10.1111/mec.13332

Rice ES, Green RE. 2019. New Approaches for Genome Assembly and Scaffolding. *Annu*

Rev Anim Biosci **7**:17–40. doi:10.1146/annurev-animal-020518-115344

Rohland N, Pollack JL, Nagel D, Beauval C, Airvaux J, Pääbo S, Hofreiter M. 2005. The population history of extant and extinct hyenas. *Mol Biol Evol* **22**:2435–2443. doi:10.1093/molbev/msi244

Roux C, Fraïsse C, Romiguier J, Anciaux Y, Galtier N, Bierne N. 2016. Shedding light on the grey zone of speciation along a continuum of genomic divergence. *PLOS Biol* **14**:e2000234. doi:10.1371/journal.pbio.2000234

Rybczynski N, Dawson MR, Tedford RH. 2009. A semi-aquatic Arctic mammalian carnivore from the Miocene epoch and origin of Pinnipedia. *Nature* **458**:1021–1024. doi:10.1038/nature07985

Sato JJ, Wolsan M, Minami S, Hosoda T, Sinaga MH, Hiyama K, Yamaguchi Y, Suzuki H. 2009. Deciphering and dating the red panda's ancestry and early adaptive radiation of Musteloidea. *Mol Phylogenet Evol* **53**:907–922. doi:10.1016/J.YMPEV.2009.08.019

Sato JJ, Wolsan M, Suzuki H, Hosoda T, Yamaguchi Y, Hiyama K, Kobayashi M, Minami S. 2006. Evidence from nuclear DNA sequences sheds light on the phylogenetic relationships of Pinnipedia: single origin with affinity to Musteloidea. *Zoolog Sci* **23**:125–146. doi:10.2108/zsj.23.125

Schröder C, Bleidorn C, Hartmann S, Tiedemann R. 2009. Occurrence of Can-SINEs and intron sequence evolution supports robust phylogeny of pinniped carnivores and their terrestrial relatives. *Gene* **448**:221–226. doi:10.1016/J.GENE.2009.06.012

Scornavacca C, Belkhir K, Lopez J, Dernat R, Delsuc F, Douzery EJP, Ranwez V. 2019. OrthoMaM v10: Scaling-up orthologous coding sequence and exon alignments with more than one hundred mammalian genomes. *Mol Biol Evol* **36**:861–862. doi:10.1093/molbev/msz015

Scott AD, Zimin A V., Puiu D, Workman R, Britton M, Zaman S, Caballero M, Read AC, Bogdanove AJ, Burns E, Wegrzyn J, Timp W, Salzberg SL, Neale DB. 2020. The giant sequoia genome and proliferation of disease resistance genes. *bioRxiv* 2020.03.17.995944. doi:10.1101/2020.03.17.995944

Shafin K, Pesout T, Lorig-Roach R, Haukness M, Olsen HE, Bosworth C, Armstrong J, Tigyi K, Maurer N, Koren S, Sedlazeck FJ, Marschall T, Mayes S, Costa V, Zook JM, Liu KJ, Kilburn D, Sorensen M, Munson KM, Vollger MR, Monlong J, Garrison E, Eichler EE, Salama S, Haussler D, Green RE, Akeson M, Phillippy A, Miga KH, Carnevali P, Jain M, Paten B. 2020. Nanopore sequencing and the Shasta toolkit enable efficient de novo assembly of eleven human genomes. *Nat Biotechnol* 1–10. doi:10.1038/s41587-020-0503-6

Shilling F, Perkins SE, Collinson W. 2015. Wildlife/Roadkill Observation and Reporting SystemsHandbook of Road Ecology. Chichester, UK: John Wiley & Sons, Ltd. pp. 492–501. doi:10.1002/9781118568170.ch62

Spitzer M, Wildenhain J, Rappsilber J, Tyers M. 2014. BoxPlotR: a web tool for generation of box plots. *Nat Methods* **11**:121–122. doi:10.1038/nmeth.2811

Srivathsan A, Baloğlu B, Wang W, Tan WX, Bertrand D, Ng AHQ, Boey EJH, Koh JJY, Nagarajan N, Meier R. 2018. A MinION™-based pipeline for fast and cost-effective

DNA barcoding. *Mol Ecol Resour* **18**:1035–1049. doi:10.1111/1755-0998.12890

Tan MH, Austin CM, Hammer MP, Lee YP, Croft LJ, Gan HM. 2018. Finding Nemo: hybrid assembly with Oxford Nanopore and Illumina reads greatly improves the clownfish (Amphiprion ocellaris) genome assembly. *Gigascience* **7**. doi:10.1093/gigascience/gix137

Tange O. 2011. Gnu parallel-the command-line power tool. *USENIX Mag* **36**:42–47.

Team R core. 2020. R: A language and environment for statistical computing.

Tilak M-K, Allio R, Delsuc F. 2020. An optimized protocol for sequencing mammalian roadkill tissues with Oxford Nanopore Technology (ONT). doi:10.17504/PROTOCOLS.IO.BEIXJCFN

Tilak M-K, Botero-Castro F, Galtier N, Nabholz B. 2018. Illumina library preparation for sequencing the GC-rich fraction of heterogeneous genomic DNA. *Genome Biol Evol* **10**:616–622. doi:10.1093/gbe/evy022

Tilak M-K, Justy F, Debiais-Thibaud M, Botero-Castro F, Delsuc F, Douzery EJP. 2015. A cost-effective straightforward protocol for shotgun Illumina libraries designed to assemble complete mitogenomes from non-model species. *Conserv Genet Resour* **7**:37–40. doi:10.1007/s12686-014-0338-x

Trauth MH, Larrasoaña JC, Mudelsee M. 2009. Trends, rhythms and events in Plio-Pleistocene African climate. *Quat Sci Rev* **28**:399–411. doi:10.1016/j.quascirev.2008.11.003

van Berkum NL, Lieberman-Aiden E, Williams L, Imakaev M, Gnirke A, Mirny LA, Dekker J, Lander ES. 2010. Hi-C: A method to study the three-dimensional architecture of genomes. *J Vis Exp* e1869. doi:10.3791/1869

van Jaarsveld AS. 1993. A comparative investigation of hyaena and aardwolf life-histories, with notes on spotted hyaena mortality patterns. *Trans R Soc South Africa* **48**:219–232. doi:10.1080/00359199309520272

Vaser R, Sović I, Nagarajan N, Šikić M. 2017. Fast and accurate de novo genome assembly from long uncorrected reads. *Genome Res* **27**:737–746. doi:10.1101/GR.214270.116

vonHoldt BM, Kays R, Pollinger JP, Wayne RK. 2016. Admixture mapping identifies introgressed genomic regions in North American canids. *Mol Ecol* **25**:2443–2453. doi:10.1111/mec.13667

Walhund S. 2010. Zusammensetzung von populationen und korrelationserscheinungen vom standpunkt der vererbungslehre aus betrachtet. *Hereditas* **11**:65–106. doi:10.1111/j.1601-5223.1928.tb02483.x

Walker BJ, Abeel T, Shea T, Priest M, Abouelliel A, Sakthikumar S, Cuomo CA, Zeng Q, Wortman J, Young SK, Earl AM. 2014. Pilon: an Integrated tool for comprehensive microbial variant detection and genome assembly improvement. *PLoS One* **9**:e112963. doi:10.1371/journal.pone.0112963

Walton LR, Joly DO. 2003. Canis mesomelas. *Mamm Species* **715**:1–9. doi:10.1644/715

Wang W, Das A, Kainer D, Schalamun M, Morales-Suarez A, Schwessinger B, Lanfear R.

2020. The draft nuclear genome assembly of Eucalyptus pauciflora: a pipeline for comparing de novo assemblies. *Gigascience* **9**. doi:10.1093/gigascience/giz160

Waterhouse RM, Seppey M, Simão FA, Manni M, Ioannidis P, Klioutchnikov G, Kriventseva E V, Zdobnov EM. 2018. BUSCO applications from quality assessments to gene prediction and phylogenomics. *Mol Biol Evol* **35**:543–548. doi:10.1093/molbev/msx319

Weisenfeld NI, Yin S, Sharpe T, Lau B, Hegarty R, Holmes L, Sogoloff B, Tabbaa D, Williams L, Russ C, Nusbaum C, Lander ES, Maccallum I, Jaffe DB. 2014. Comprehensive variation discovery in single human genomes. *Nat Genet* **46**:1350–1355. doi:10.1038/ng.3121

Wenger AM, Peluso P, Rowell WJ, Chang P-C, Hall RJ, Concepcion GT, Ebler J, Fungtammasan A, Kolesnikov A, Olson ND, Töpfer A, Alonge M, Mahmoud M, Qian Y, Chin C-S, Phillippy AM, Schatz MC, Myers G, DePristo MA, Ruan J, Marschall T, Sedlazeck FJ, Zook JM, Li H, Koren S, Carroll A, Rank DR, Hunkapiller MW. 2019. Accurate circular consensus long-read sequencing improves variant detection and assembly of a human genome. *Nat Biotechnol* **37**:1155–1162. doi:10.1038/s41587-019-0217-9

Westbury M V, Hartmann S, Barlow A, Wiesel I, Leo V, Welch R, Parker DM, Sicks F, Ludwig A, Dalén L, Hofreiter M. 2018. Extended and continuous decline in effective population size results in low genomic diversity in the world's rarest hyena species, the brown hyena. *Mol Biol Evol* **35**:1225–1237. doi:10.1093/molbev/msy037

Wick RR, Judd LM, Holt KE. 2019. Performance of neural network basecalling tools for Oxford Nanopore sequencing. *Genome Biol* **20**:129. doi:10.1186/s13059-019-1727-y

Wickham H. 2016. Ggplot2 : elegant graphics for data analysis. Springer.

Wilke CO. 2016. cowplot: Streamlined plot theme and plot annotations for "ggplot2." *CRAN Repos*.

Wilson DE, Mittermeier RA, Cavallini P. 2009. Handbook of the mammals of the world, Vol. 1. ed. Barcelona: Lynx Edicions.

Zdobnov EM, Tegenfeldt F, Kuznetsov D, Waterhouse RM, Simão FA, Ioannidis P, Seppey M, Loetscher A, Kriventseva E V. 2017. OrthoDB v9.1: cataloging evolutionary and functional annotations for animal, fungal, plant, archaeal, bacterial and viral orthologs. *Nucleic Acids Res* **45**:D744–D749. doi:10.1093/nar/gkw1119

Zhang C, Rabiee M, Sayyari E, Mirarab S. 2018. ASTRAL-III: polynomial time species tree reconstruction from partially resolved gene trees. *BMC Bioinforma 2018 196* **19**:15–30. doi:10.1186/s12859-018-2129-y

Zimin A V., Marçais G, Puiu D, Roberts M, Salzberg SL, Yorke JA. 2013. The MaSuRCA genome assembler. *Bioinformatics* **29**:2669–2677. doi:10.1093/bioinformatics/btt476

Zimin A V., Puiu D, Luo M-C, Zhu T, Koren S, Marçais G, Yorke JA, Dvořák J, Salzberg SL. 2017. Hybrid assembly of the large and highly repetitive genome of Aegilops tauschii, a progenitor of bread wheat, with the MaSuRCA mega-reads algorithm. *Genome Res* **27**:787–792. doi:10.1101/GR.213405.116

Additional files

Figure S1: Plot of the quality of Nanopore long reads base-called with either the *fast* or the *high accuracy* option of Guppy v3.1.5. The quality of the base-calling step has a large impact on the final quality of the assemblies by reducing the number of contigs and increasing the N50 value.

Figure S2: Definition of the genetic differentiation index (GDI) based on the F-statistic (FST). The main difference between these two indexes is the use of heterozygous allele states for GDI rather than real polymorphism for the FST. Green = π_{within}, Orange = $\pi_{between}$, Blue = Population A, Red = Population A+B.

Figure S3: Graphical representation of the results of contamination analyses performed with BlobTools for a) the aardwolf (*Proteles cristata*) and b) the bat-eared fox (*Otocyon megalotis*).

Table S1: Pairwise patristic distances estimated for the 142 species based on the phylogenetic tree inferred with the 15 mitochondrial loci (2 rRNAs and 13 protein-coding genes).

Table S2: Results of Bayesian dating for the two nodes leading to the *Proteles cristata* spp. and the *Otocyon megalotis* spp.. Divergence time estimates based on UGAM and LN models are reported with associated 95% credibility intervals for each MCMC chain.

Table S3: Sample details and assembly statistics (Number of contigs/scaffolds and associated N50 values) for the 503 mammalian assemblies retrieved from NCBI (https://www.ncbi.nlm.nih.gov/assembly) on August 13th, 2019 with filters: "Exclude derived from surveillance project", "Exclude anomalous", "Exclude partial", and using only the RefSeq assembly for *Homo sapiens*.

Table S4: Genome completeness assessment of MaSuRCA and SOAPdenovo assemblies obtained for *Proteles cristata* and *Otocyon megalotis* together with the 63 carnivore assemblies available at NCBI and DNAZoo (https://www.dnazoo.org/assemblies) on August 13th, 2019 using Benchmarking Universal Single-Copy Orthologs (BUSCO) v3 with the Mammalia OrthoDB 9 BUSCO gene set.

Table S5: Annotation summary and supermatrix composition statistics of the 53 species used to infer the genome-scale Carnivora phylogeny.

Table S6. Sample details, Illumina sequencing, and assembly statistics of the 10 newly assembled carnivoran mitochondrial genomes.

Table S7: Node calibrations used for the Bayesian dating inferences based on mitogenomic data.

Table S8: Results of contamination analyses performed with BlobTools for the aardwolf (*Proteles cristata*).

Table S9: Results of contamination analyses performed with BlobTools for the bat-eared fox (*Otocyon megalotis*).

Table S10: Summary information for the Carnivora genomes available either on Genbank, DNAZoo (https://www.dnazoo.org) and the OrthoMaM database as of February 11th, 2020. The "OMM" column indicates if the genome was available on OMM (yes) or not (no). The "Annotation" column indicates whether the genome was already annotated (yes) or not (no).

Supplementary Figures and Tables

for

High-quality carnivore genomes from roadkill samples enable species delimitation in aardwolf and bat-eared fox

Rémi Allio[1*], Marie-Ka Tilak[1], Céline Scornavacca[1], Nico L. Avenant[2], Erwan Corre[3], Benoit Nabholz[1], and Frédéric Delsuc[1*]

[1]Institut des Sciences de l'Evolution de Montpellier (ISEM), CNRS, IRD, EPHE, Université de Montpellier, France remi.allio@umontpellier.fr marie-ka.tilak@umontpellier.fr celine.scornavacca@umontpellier.fr benoit.nabholz@umontpellier.fr frederic.delsuc@umontpellier.fr

[2]National Museum and Centre for Environmental Management, University of the Free State, Bloemfontein, South Africa navenant@nasmus.co.za

[3]CNRS, Sorbonne Université, FR2424, ABiMS, Station Biologique de Roscoff, 29680 Roscoff, France corre@sb-roscoff.fr

[*]Correspondence: remi.allio@umontpellier.fr, frederic.delsuc@umontpellier.fr

Figure S1: Plot of the quality of Nanopore long reads base-called with either the *fast* or the *high accuracy* option of Guppy v3.1.5. The quality of the base-calling step has a large impact on the final quality of the assemblies by reducing the number of contigs and increasing the N50 value.

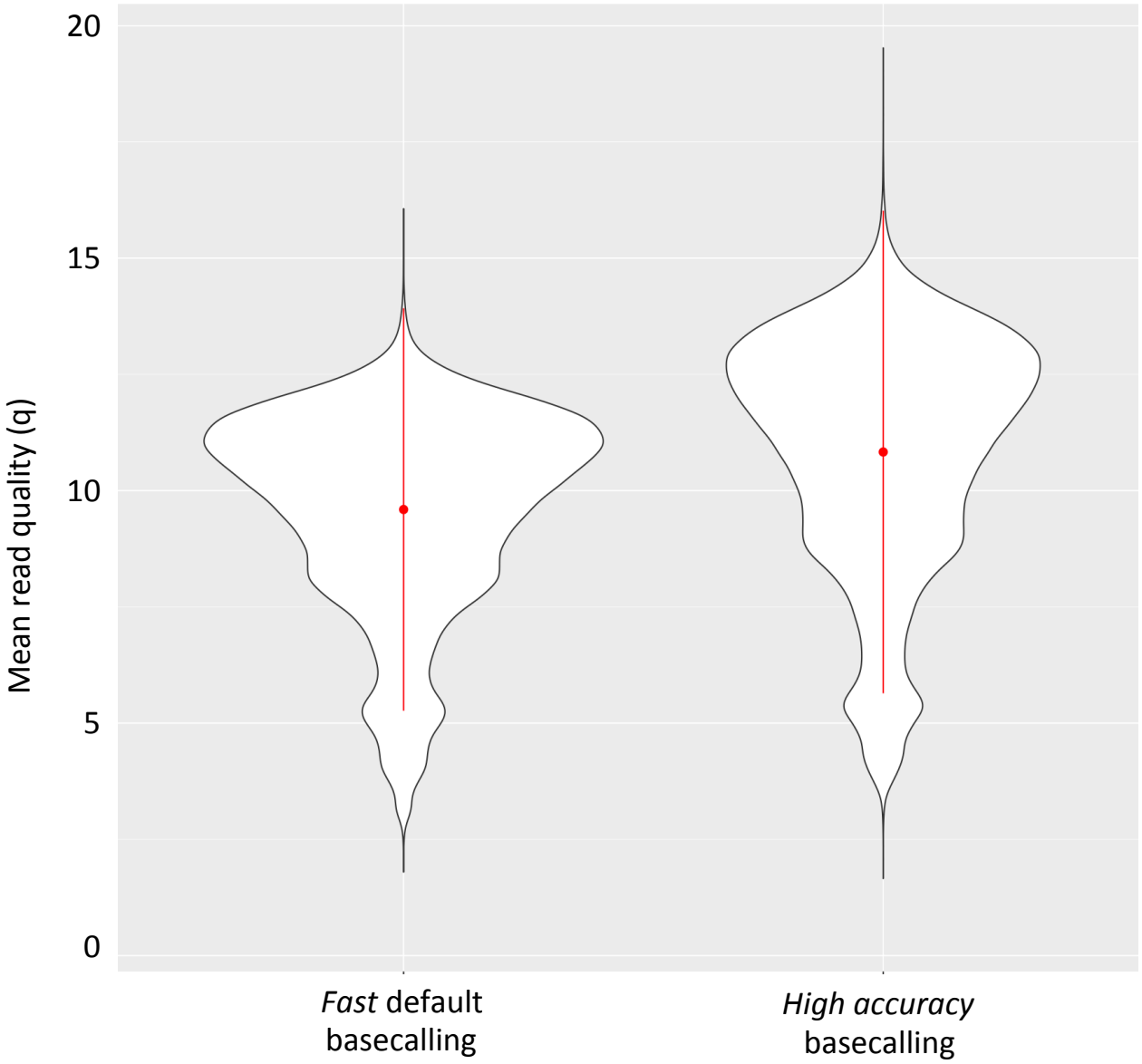

Aardwolf

Fast default basecalling		*High accuracy* basecalling
Contigs: 8,874	→	5,669
N50: 699 Kb	→	1.31 Mb

Bat-eared fox

Fast default basecalling		*Higher accuracy* basecalling
Contigs: 12,735	→	11,081
N50: 676 Kb	→	728 Kb

Figure S2: Definition of the genetic differentiation index (GDI) based on the F-statistic (FST). The main difference between these two indexes is the use of heterozygous allele states for GDI rather than real polymorphism for the FST. Green = π_{within}, Orange = $\pi_{between}$, Blue = Population A, Red = Population A+B.

F-Stastistic:

$$\mathbf{FST} = 1 - \frac{\pi_{within}}{\pi_{between}}$$

Hudson et al 1992

FST = 1 = Highly structured
FST = 0 = No structuration

Genetic differentiation index (GDI, based on heterozygosity):

Fixed	Private A	Private B	Shared
AA/TT	AT/AA	AA/AT	AT/AT

π_{AB} = fixed + $private_A$ + $private_B$ + $shared_{AB}$
π_A = $private_A$ + $shared_{AB}$
π_B = $private_B$ + $shared_{AB}$

$$1 - \frac{(\pi_A + \pi_B)/2}{\pi_{tot\ AB}}$$

For different population level:

$$1 - \frac{(\pi_{A1} + \pi_{A2})/2}{\pi_{tot\ A}} \quad \text{vs} \quad 1 - \frac{(\pi_{A1} + \pi_{B1})/2}{\pi_{tot\ A1B1}}$$

GDI within pop A (control)

global GDI

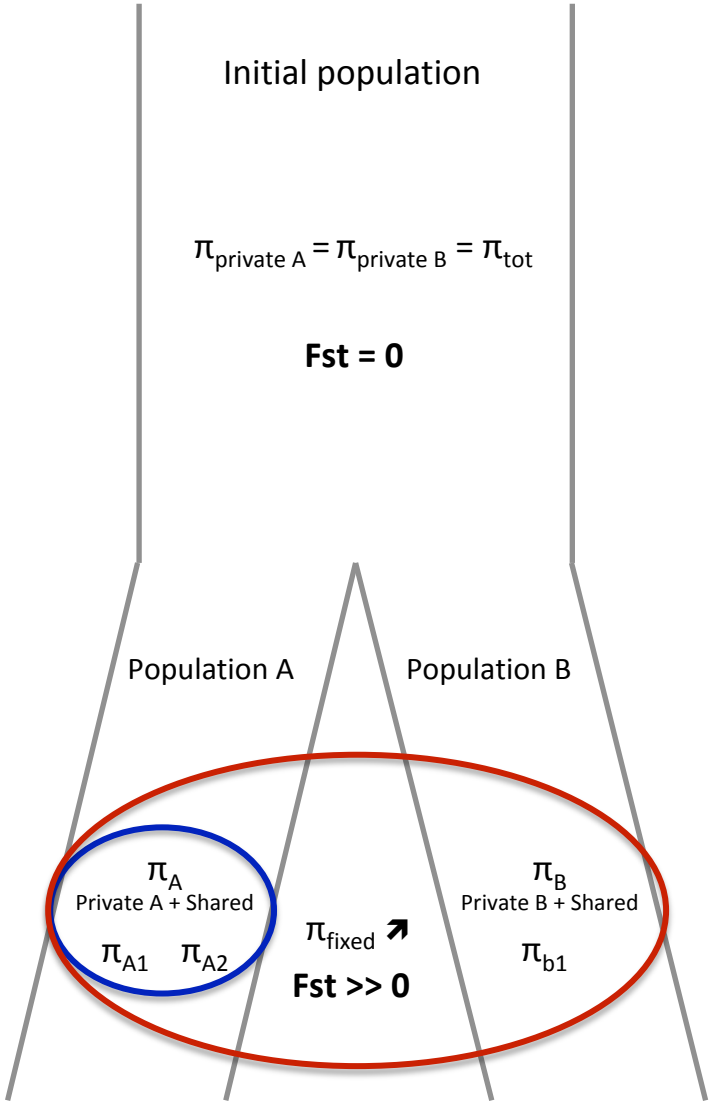

Figure S3: Graphical representation of the results of contamination analyses performed with BlobTools for a) the aardwolf (*Proteles cristata*) and b) the bat-eared fox (*Otocyon megalotis*).

a) BlobTools results for *Proteles cristatus*

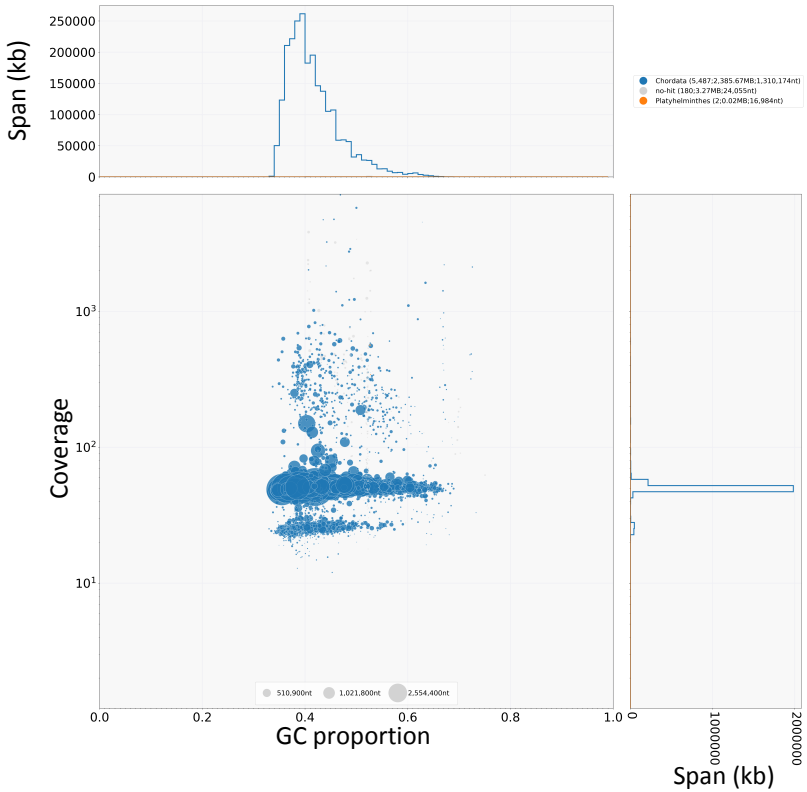

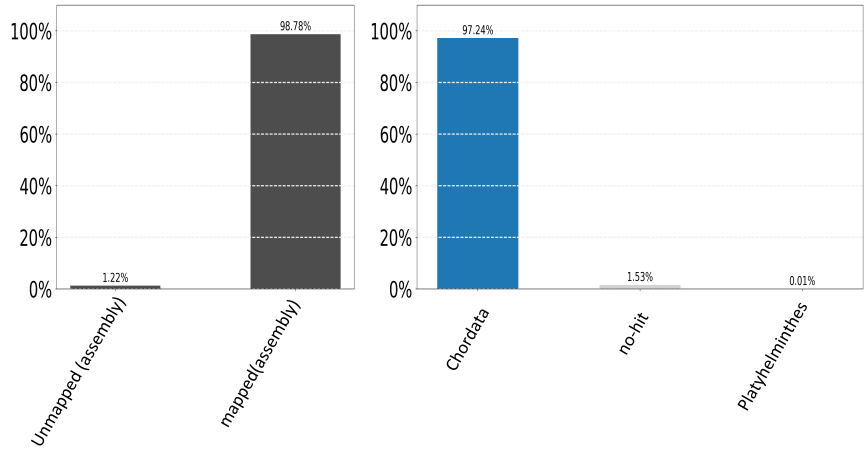

b) BlobTools results for *Otocyon megalotis*

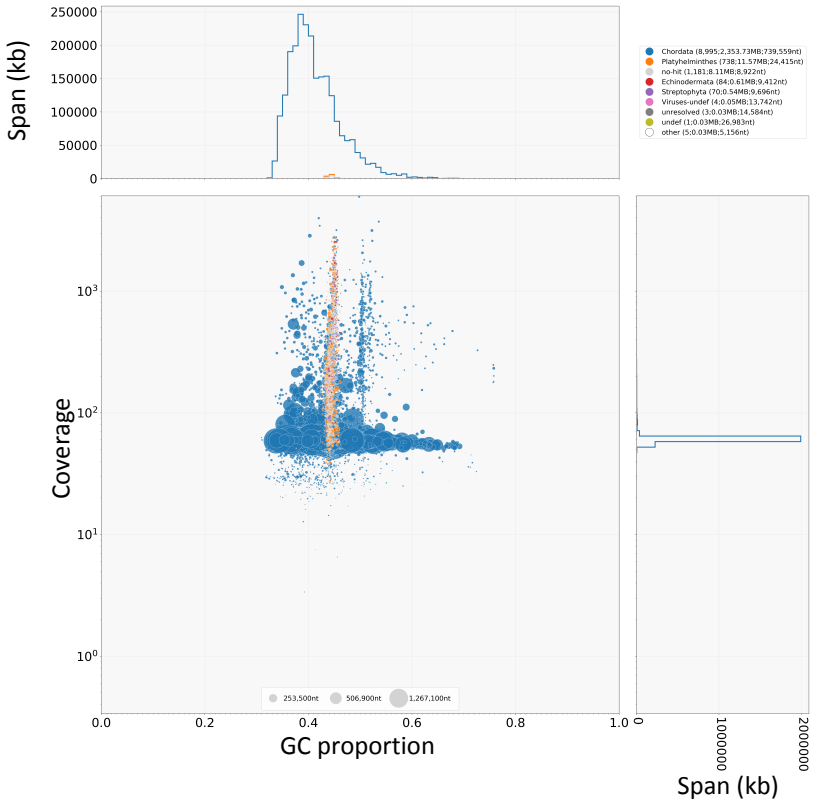

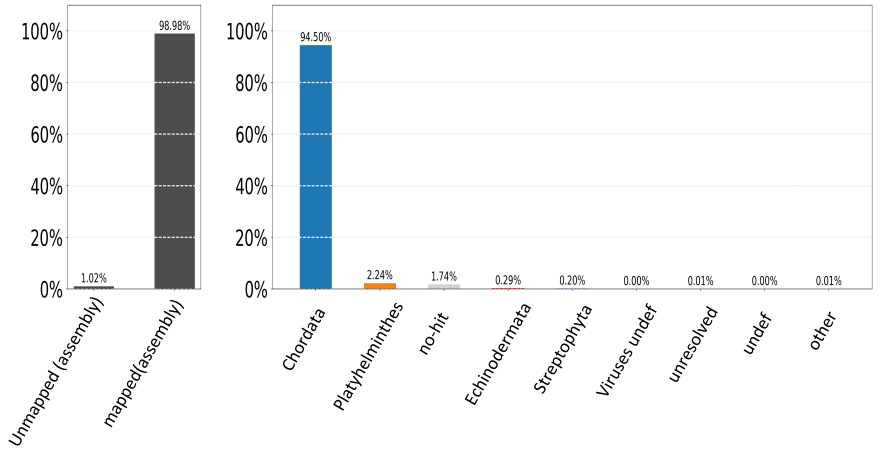

Table S1: Pairwise patristic distances estimated for the 142 species based on the phylogenetic tree inferred with the 15 mitochondrial loci (2 rRNAs and 13 protein-coding genes).

SEE XLS FILES

Table S2: Results of Bayesian dating for the two nodes leading to the *Proteles cristata* spp. and the *Otocyon megalotis* spp.. Divergence time estimates based on UGAM and LN models are reported with associated 95% credibility intervals for each MCMC chain.

Species pair	LN			UGAM		
	Chain 1	Chain 2	Chain 3	Chain 1	Chain 2	Chain 3
Proteles cristata/ Proteles septentrionalis	1.228 [IC 95%: 5.34 – 0.58]	1.014 [IC 95%: 3.01 – 0.56]	0.841 [IC 95%: 1.26 – 0.55]	1.327 [IC 95%: 1.86 – 0.93]	1.335 [IC 95%: 1.86 – 0.94]	1.34 [IC 95%: 1.88 – 0.94]
Otocyon megalotis megalotis/ Otocyon megalotis virgatus	1.295 [IC 95%: 6.72 – 0.43]	1.007 [IC 95%: 2.61 – 0.52]	0.865 [IC 95%: 1.45– 0.48]	0.569 [IC 95%: 0.81 – 0.39]	0.573 [IC 95%: 0.83 – 0.39]	0.57 [IC 95%: 0.82 – 0.40]

Table S3: Sample details and assembly statistics (Number of contigs/scaffolds and associated N50 values) for the 503 mammalian assemblies retrieved from NCBI (https://www.ncbi.nlm.nih.gov/assembly) on August 13th, 2019 with filters: "Exclude derived from surveillance project", "Exclude anomalous", "Exclude partial", and using only the RefSeq assembly for *Homo sapiens*.

SEE XLS FILES

Table S4: Genome completeness assessment of MaSuRCA and SOAPdenovo assemblies obtained for *Proteles cristata* and *Otocyon megalotis* together with the 63 carnivore assemblies available at NCBI and DNAZoo (https://www.dnazoo.org/assemblies) on August 13th, 2019 using Benchmarking Universal Single-Copy Orthologs (BUSCO) v3 with the Mammalia OrthoDB 9 BUSCO gene set.

SEE XLS FILES

Table S5: Annotation summary and supermatrix composition statistics of the 53 species used to infer the genome-scale Carnivora phylogeny.

Species	Maker annotated genes	Number of orthologous genes after cleaning	Missing data
Acinonyx_jubatus	NA	12751	16.54
Ailuropoda_melanoleuca	NA	13411	9.57
Ailurus_fulgens	17619	11675	26.14
Arctocephalus_gazella	13714	8390	60.29
Bassariscus_sumichrasti	17573	11713	26.97
Callorhinus_ursinus	46164	7398	53.35
Canis_lupus_familiaris	NA	13808	6.04
Crocuta_Crocuta	16828	11525	29.17
Cryptoprocta_ferox	18199	12244	20.82
Enhydra_lutris	NA	13746	4.67
Eumetopias_jubatus	39926	8515	46.70
Felis_catus	NA	13047	11.98
Gulo_gulo	19696	8939	48.42
Helogale_parvula	18484	12005	23.92
Hyaena_hyaena	17663	12169	22.27
Leptonychotes_weddellii	NA	12439	22.57
Lutra_lutra	32278	12304	19.89
Lycaon_pictus	18068	11405	27.75
Lynx_canadensis	44864	7203	56.76
Lynx_pardinus	31025	9961	39.55
Manis_javanica	NA	12441	18.81
Mellivora_capensis	18194	12146	22.63
Mirounga_angustirostris	32777	12305	19.37
Mungos_mungo	18832	12241	21.30
Mustela_putorius	NA	13172	8.70
Nasua_narica	16858	11442	29.08
Neofelis_nebulosa	29785	12614	18.28
Neomonachus_schauinslandi	NA	13690	5.80
Neovison_vison	17294	11848	26.03
Odobenus_rosmarus	NA	13705	5.14
Otocyon_megalotis	18996	11981	22.02
Panthera_leo	17539	12162	22.91
Panthera_onca	16942	11758	27.22
Panthera_pardus	NA	13731	5.49
Panthera_tigris	NA	12841	15.37
Paradoxurus_hermaphroditus	17278	11387	30.18
Phoca_vitulina	18387	12057	22.73
Potos_flavus	27890	12234	22.80
Prionailurus_bengalensis	18057	12172	22.88
Procyon_lotor	16572	11165	32.46
Proteles_septentrionalis	NA	12050	22.43
Proteles_cristatus	17570	12062	22.96
Pteronura_brasiliensis	18445	12332	20.62
Puma_concolor	23358	10853	28.62
Spilogale_gracilis	17606	11744	26.61
Suricata_suricatta	17398	11707	26.32
Taxidea_taxus	15586	10141	42.19
Ursus_americanus	17694	11670	27.53
Ursus_arctos	18003	12145	22.21
Ursus_maritimus	NA	13111	13.56
Ursus_thibetanus	18365	12092	22.87
Vulpes_vulpes	18511	11688	26.02
Zalophus_californianus	NA	6305	64.65

Table S6. Sample details, Illumina sequencing, and assembly statistics of the 10 newly assembled carnivoran mitochondrial genomes.

Species	Common name	Collection number	Origin	Sample type	Raw reads	Mito reads	Mean coverage	SRA Accession	Genbank Accession
Proteles cristata cristata	Southern aardwolf	NMB (TS307)	South Africa	Tissue	4,779,321	6,665	39x	Pending	Pending
Proteles cristata septentrionalis	Eastern aardwolf	NMS Z.2018.54	Tanzania	Tissue	7,597,504	2,709	19x	Pending	Pending
Otocyon megalotis megalotis	Southern bat-eared fox	NMB (TS305)	South Africa	Tissue	6,719,302	4,559	27x	Pending	Pending
Otocyon megalotis virgatus	Eastern bat-eared fox	FMNH 158128	Tanzania	Tissue	6,838,309	37,719	219x	Pending	Pending
Speothos venaticus	Bush dog	ISEM T1624	French Guiana	Tissue	5,271,782	4,763	27x	Pending	Pending
Vulpes vulpes	Red fox	ISEM T3611	France	Tissue	8,355,398	3,050	18x	Pending	Pending
Parahyaena brunnea	Brown hyaena	ISEM FD126	Toulon Zoo	Feces	11,739,905	3,243	17x	Pending	Pending
Bdeogale nigripes	Black-footed mongoose	FMNH 167685	Gabon	Tissue	6,839,178	8,215	61x	SRR6053065*	Pending
Fossa fossana	Malagasy civet	FMNH 156648	Madagascar	Tissue	4,914,258	17,689	131x	SRR6053060*	Pending
Viverra tangalunga	Malayan civet	FMNH 146957	Philippines	Tissue	5,648,442	23,116	205x	SRR6053069*	Pending

*: UCE capture reads from Esselstyn et al. (2017); NMB: National Museum, Bloemfontein, South Africa; ISEM: Institut des Sciences de l'Evolution, Montpellier, France; FMNH: Field Museum of Natural History, Chicago, IL, USA.

Table S7: Node calibrations used for the Bayesian dating inferences based on mitogenomic data.

Node	upper limit (My)	lower limit (My)
Felis_catus,Lynx_lynx	NA	5.3
Felis_catus,Panthera_onca	16.4	NA
Felis_catus,Prionodon_pardicolor	NA	28.5
Proteles_cristatus_cristatus_TS307,Hyaena_hyaena	16.4	NA
Urva_javanica,Fossa_fossana_FMNH156648_SRR6053060	NA	16.4
Proteles_cristatus_cristatus_TS307,Urva_javanica	NA	16.4
Civettictis_civetta,Genetta_servalina	NA	11.2
Canis_lupus,Urocyon_cinereoargenteus	NA	5.3
Mephitis_mephitis,Spilogale_putorius	NA	1.8
Procyon_lotor,Nasua_nasua	NA	11.2
Nasua_nasua,Ailurus_fulgens	NA	16.4
Arctocephalus_pusillus,Zalophus_californianus	NA	1.8
Mirounga_leonina,Phoca_fasciata	NA	11.2
Arctocephalus_pusillus,Phoca_fasciata	NA	16.4
Arctocephalus_pusillus,Nasua_nasua	NA	28.5
Ursus_arctos,Ailuropoda_melanoleuca	NA	3.5
Canis_lupus,Ursus_arctos	NA	37
Felis_catus,Canis_lupus	65.8	50

Table S8: Results of contamination analyses performed with BlobTools for the aardwolf (*Proteles cristata*).

Table S9: Results of contamination analyses performed with BlobTools for the bat-eared fox (*Otocyon megalotis*).

SEE XLS FILES

Table S10: Summary information for the Carnivora genomes available either on Genbank, DNAZoo (https://www.dnazoo.org) and the OrthoMaM database as of February 11th, 2020. The "OMM" column indicates if the genome was available on OMM (yes) or not (no). The "Annotation" column indicates whether the genome was already annotated (yes) or not (no).

Species	Order	Family	Accession	AssemblyName	Database	Assembly	Busco scores					OMM	Annotation
							Complete	Fragmented	Missing	Single	Duplicated		
Acinonyx jubatus	Carnivora	Felidae	GCF_001443585.1	aciJub1	NCBI	Acinonyx jubatus [aciJub1]	90.5	6.0	3.5	90.2	0.3	Yes	Yes
Ailuropoda melanoleuca	Carnivora	Ursidae	GCF_000004335.2	AilMel_1.0	NCBI	Ailuropoda melanoleuca [AilMel_1.0]	92.9	4.6	2.5	92.6	0.3	Yes	Yes
Ailurus fulgens	Carnivora	Ailuridae	ASM200746v1_DNAZoo_HiC	ASM200746v1_DNAZoo_HiC	DNAZoo	Ailurus fulgens [ASM200746v1_DNAZoo_HiC]	95.4	2.3	2.3	94.6	0.8	No	Yes
Arctocephalus gazella	Carnivora	Otariidae	GCA_900500725.1	ArcGazv1.4	NCBI	Arctocephalus gazella [ArcGazv1.4]	81.6	12.4	6.0	80.8	0.8	No	No
Callorhinus ursinus	Carnivora	Otariidae	GCF_003265705.1	ASM326570v1	NCBI	Callorhinus ursinus [ASM326570v1]	93.0	3.6	3.4	81.2	11.8	No	Yes
Canis lupus	Carnivora	Canidae	GCF_000002285.3	CanFam3.1	NCBI	Canis lupus [CanFam3.1]	95.3	2.4	2.3	94.0	1.3	Yes	Yes
Crocuta crocuta	Carnivora	Hyaenidae	GCA_008692635.1	BGI_CrCroc_1.0	NCBI	Crocuta crocuta [BGI_CrCroc_1.0]	95.5	2.5	2.0	95.0	0.5	No	No
Cryptoprocta ferox	Carnivora	Eupleridae	GCA_004023885.1	CryFer_v1_BIUU	NCBI	Cryptoprocta ferox [CryFer_v1_BIUU]	85.9	10.6	3.5	84.9	1.0	No	No
Enhydra lutris	Carnivora	Mustelidae	GCF_002288905.1	ASM228890v2	NCBI	Enhydra lutris [ASM228890v2]	94.2	3.5	2.3	93.2	1.0	Yes	Yes
Eumetopias jubatus	Carnivora	Otariidae	GCF_004028035.1	ASM402803v1	NCBI	Eumetopias jubatus [ASM402803v1]	93.4	3.7	2.9	91.2	2.2	No	Yes
Felis catus	Carnivora	Felidae	GCF_000181335.3	Felis_catus_9.0	NCBI	Felis catus [Felis_catus_9]	93.1	3.8	3.1	92.7	0.4	Yes	Yes
Gulo gulo	Carnivora	Mustelidae	GCA_900006375.2	Gulo_2.2_annotated	NCBI	Gulo gulo [Gulo_2.2]	85.4	10.6	4.0	85.0	0.4	No	Yes
Helogale parvula	Carnivora	Herpestidae	GCA_004023845.1	HelPar_v1_BIUU	NCBI	Helogale parvula [HelPar_v1_BIUU]	83.9	11.8	4.3	83.2	0.7	No	No
Hyaena hyaena	Carnivora	Hyaenidae	GCA_003009895.1	ASM300989v1	NCBI	Hyaena hyaena [ASM300989v1]	93.5	4.0	2.5	92.8	0.7	No	No
Leptonychotes weddellii	Carnivora	Phocidae	GCF_000349705.1	LepWed1.0	NCBI	Leptonychotes weddellii [LepWed1.0]	78.8	15.3	5.9	77.8	1.0	Yes	Yes
Lutra lutra	Carnivora	Mustelidae	mLutLut1_DNAZoo_HiC	mLutLut1_DNAZoo_HiC	DNAZoo	Lutra lutra [mLutLut1_DNAZoo_HiC]	95.5	2.2	2.3	94.1	1.4	No	Yes
Lycaon pictus	Carnivora	Canidae	sis2-181106_DNAZoo_HiC	sis2-181106_DNAZoo_HiC	DNAZoo	Lycaon pictus [sis2-181106_DNAZoo_HiC]	94.7	2.5	2.8	93.5	1.2	No	Yes
Lynx canadensis	Carnivora	Felidae	GCA_007474595.1	mLynCan4_v1.p	NCBI	Lynx canadensis [mLynCan4_v1.p_VGP]	94.6	2.7	2.7	94.2	0.4	No	Yes
Lynx pardinus	Carnivora	Felidae	GCA_900661375.1	LYPA1.0	NCBI	Lynx pardinus [LYPA1.0]	94.4	3.1	2.5	93.9	0.5	No	Yes
Mellivora capensis	Carnivora	Mustelidae	GCA_004024625.1	MelCap_v1_BIUU	NCBI	Mellivora capensis [MelCap_v1_BIUU]	78.2	16.1	5.7	77.7	0.5	No	No
Mirounga angustirostris	Carnivora	Phocidae	Mirounga_angustirostris_DNAZoo_HiC	Mirounga_angustirostris_DNAZoo_HiC	DNAZoo	Mirounga angustirostris [Mirounga_angustirostris_DNAZoo_HiC]	94.7	2.8	2.5	93.7	1.0	No	Yes
Mungos mungo	Carnivora	Herpestidae	GCA_004023785.1	MunMun_v1_BIUU	NCBI	Mungos mungo [MunMun_v1_BIUU]	87.4	9.1	3.5	86.6	0.8	No	No
Mustela putorius	Carnivora	Mustelidae	GCF_000215625.1	MusPutFur1.0	NCBI	Mustela putorius [MusPutFur1.0]	93.5	3.9	2.6	92.9	0.6	Yes	Yes
Nasua narica	Carnivora	Procyonidae	Nasua_narica_DNAZoo_HiC	Nasua_narica_DNAZoo_HiC	DNAZoo	Nasua narica [Nasua_narica_DNAZoo_HiC]	90.7	5.0	4.3	90.1	0.6	No	No
Neofelis nebulosa	Carnivora	Felidae	Neofelis_nebulosa_DNAZoo_HiC	Neofelis_nebulosa_DNAZoo_HiC	DNAZoo	Neofelis nebulosa [Neofelis_nebulosa_DNAZoo_HiC]	95.8	1.9	2.3	95.1	0.7	No	Yes
Neomonachus schauinslandi	Carnivora	Phocidae	GCF_002201575.1	ASM220157v1	NCBI	Neomonachus schauinslandi [ASM220157v1]	93.0	4.3	2.7	91.9	1.1	Yes	Yes
Neovison vison	Carnivora	Mustelidae	GCA_900108605.1	NNQGG.v01	NCBI	Neovison vison [NNQGG.v01]	94.0	3.8	2.2	93.4	0.6	No	No
Odobenus rosmarus	Carnivora	Odobenidae	GCF_000321225.1	Oros_1.0	NCBI	Odobenus rosmarus [Oros_1.0]	93.4	3.8	2.8	91.9	1.5	Yes	Yes
Otocyon megalotis	Carnivora	Canidae	ISEM_TS305_MaSuRCA	Otoc_meg_TS305_MaSuRCA	ISEM	Otocyon megalotis [ISEM_TS305_MaSuRCA]	92.9	4.2	2.9	91.7	1.2	No	Yes
Panthera leo	Carnivora	Felidae	GCA_008795835.1	PanLeo1.0	NCBI	Panthera leo [PanLeo1.0]	96.2	1.9	1.9	95.6	0.6	No	No
Panthera onca	Carnivora	Felidae	GCA_004023805.1	PanOnc_v1_BIUU	NCBI	Panthera onca [PanOnc_v1_BIUU]	78.4	15.7	5.9	78.0	0.4	No	No
Panthera pardus	Carnivora	Felidae	GCF_001857705.1	PanPar1.0	NCBI	Panthera pardus [PanPar1.0]	93.5	3.8	2.7	92.7	0.8	Yes	Yes
Panthera tigris	Carnivora	Felidae	GCF_000464555.1	PanTig1.0	NCBI	Panthera tigris [PanTig1.0]	91.5	5.3	3.2	91.2	0.3	Yes	Yes
Paradoxurus hermaphroditus	Carnivora	Viverridae	GCA_004024585.1	ParHer_v1_BIUU	NCBI	Paradoxurus hermaphroditus [ParHer_v1_BIUU]	74.8	18.4	6.8	74.2	0.6	No	No
Phoca vitulina	Carnivora	Phocidae	GSC_HSeal_1.0_DNAZoo_HiC	GSC_HSeal_1.0_DNAZoo_HiC	DNAZoo	Phoca vitulina [GSC_HSeal_1.0_DNAZoo_HiC]	95.2	2.3	2.5	94.1	1.1	No	Yes
Potos flavus	Carnivora	Procyonidae	Potos_flavus_DNAZoo_HiC	Potos_flavus_DNAZoo_HiC	DNAZoo	Potos flavus [Potos_flavus_DNAZoo_HiC]	92.7	4.4	2.9	92.2	0.5	No	Yes
Prionailurus bengalensis	Carnivora	Felidae	GCA_005406085.1	Prionailurus_bengalensis_euptilurus_v01	NCBI	Prionailurus bengalensis [Prionailurus_bengalensis_euptilurus_v01]	84.2	11.0	4.8	83.7	0.5	No	No
Procyon lotor	Carnivora	Procyonidae	pl-1k_DNAZoo_HiC	pl-1k_DNAZoo_HiC	DNAZoo	Procyon lotor [pl-1k_DNAZoo_HiC]	87.8	7.2	5.0	87.2	0.6	No	Yes
Proteles cristatus	Carnivora	Hyaenidae	ISEM_TS307_MaSuRCA	Prot_cri_TS307_MaSuRCA	ISEM	Proteles cristatus [ISEM_TS307_MaSuRCA]	92.8	3.8	3.4	92.3	0.5	No	Yes
Pteronura brasiliensis	Carnivora	Mustelidae	GCA_004024605.1	PteBra_v1_BIUU	NCBI	Pteronura brasiliensis [PteBra_v1_BIUU]	82.0	13.3	4.7	81.4	0.6	No	No
Puma concolor	Carnivora	Felidae	GCF_003327715.1	PumCon1.0	NCBI	Puma concolor [PumCon1]	93.4	3.4	3.2	93.0	0.4	No	Yes
Spilogale gracilis	Carnivora	Mephitidae	GCA_004023965.1	SpiGra_v1_BIUU	NCBI	Spilogale gracilis [SpiGra_v1_BIUU]	76.7	17.1	6.2	76.1	0.6	No	No
Suricata suricatta	Carnivora	Herpestidae	GCF_006229205.1	meerkat_22Aug2017_6uvM2_HiC	DNAZoo	Suricata suricatta [meerkat_22Aug2017_6uvM2_DNAZoo_HiC]	94.7	2.6	2.7	93.5	1.2	No	Yes
Taxidea taxus	Carnivora	Mustelidae	GCA_003697995.1	ASM369799v1	NCBI	Taxidea taxus [ASM369799v1]	58.5	28.4	13.1	57.5	1.0	No	No
Ursus americanus	Carnivora	Ursidae	ASM334442v1_DNAZoo_HiC	ASM334442v1_DNAZoo_HiC	DNAZoo	Ursus americanus [ASM334442v1_DNAZoo_HiC]	93.9	3.3	2.8	93.3	0.6	No	Yes
Ursus arctos	Carnivora	Ursidae	ASM358476v1_DNAZoo_HiC	ASM358476v1_DNAZoo_HiC	DNAZoo	Ursus arctos [ASM358476v1_DNAZoo_HiC]	95.7	2.0	2.3	94.8	0.9	No	Yes
Ursus maritimus	Carnivora	Ursidae	GCF_000687225.1	UrsMar_1.0	NCBI	Ursus maritimus [UrsMar_1]	91.8	5.5	2.7	91.4	0.4	Yes	Yes
Ursus thibetanus	Carnivora	Ursidae	GCA_009660055.1	ASM966005v1	NCBI	Ursus thibetanus [ASM966005v1]	95.8	1.8	2.4	94.4	1.4	No	No
Vulpes vulpes	Carnivora	Canidae	VulVul2.2_DNAZoo_HiC	VulVul2.2_DNAZoo_HiC	NCBI	Vulpes vulpes [VulVul2.2_DNAZoo_HiC]	94.7	2.8	2.5	93.3	1.4	No	Yes
Zalophus californianus	Carnivora	Otariidae	GCF_900631625.1	zalCal2.2	NCBI	Zalophus californianus [zalCal2.2]	93.3	3.7	3.0	91.8	1.5	No	Yes